銖元素添加對鎳基 Mar-M247 超合金顯微組織及機械性能之影響

研究生：廖健鴻　　指導教授：劉 增 豐 博士

國立交通大學材料科學與工程研究所

中文摘要

本論文旨在探討銖元素添加對鎳基Mar-M247 超合金顯微組織及機械性能之影響。實驗結果顯示Mar-M247 超合金中添加銖元素含量為 0、1、3、5 wt.%時，其晶粒尺寸分別為 90、70、60、50μm。隨著銖含量之增加，一次γ′相被細化及立方體化會越為顯著。在γ晶粒內之長條狀MC碳化物中的鉭及鈦含量，會隨著合金中銖含量的增加而逐漸減少。當添加 3 wt.%銖元素時，晶粒內長條狀MC碳化物會分解成不連續狀$M_{23}C_6$碳化物，且少量拓撲密堆(TCP)有害相會開始在晶粒內形成。當銖含量增加至 5 wt.%時，會因銖及鎢等元素嚴重的偏析，增加顯微組織之不穩定性，導致大量針狀P相在晶粒內形成。

室溫至中溫(760℃)拉伸測試結果顯示，添加 3 wt.%銖可顯著提昇抗拉及降伏強度。760℃/724MPa 潛變測試結果顯示，潛變性質主要由穩態潛變(潛變第二階段)所控制。與未添加銖元素合金相較，含 3 wt.%銖之合金其穩態潛變速率下降約 31%，而潛變壽命延長約 63%。微硬度測試結果顯示，銖

的添加具有提高 γ/γ′基地強度的效果，其中又以含 3 wt.%銖合金之 γ/γ′基地強度最強。含 3 wt.%銖之 Mar-M247 超合金其拉伸及潛變性能的提昇是因為銖具有細化晶粒及提昇 γ/γ′基地強度的效果。然而，添加 5 wt.%銖，會因晶粒內大量針狀 P 相的形成，造成拉伸及潛變性能的下降。破斷面分析結果顯示，Mar-M247 超合金中銖元素含量為 0–3 wt.%時，其拉伸及潛變之破裂模式是沿晶破裂；而銖含量為 5 wt.%時，其拉伸及潛變之破裂模式是裂縫沿著晶界及針狀 P 相成長。

982℃拉伸及 982℃/200MPa 潛變測試結果顯示，拉伸性能及潛變壽命會隨著銖在 Mar-M247 超合金中含量的增加而提昇，至 3 wt.%銖含量時達到最大值。針對晶界碳化物形貌統計分析結果顯示，隨著銖含量增加，晶界碳化物的尺寸會變的越小而其數量會變的越多，而此晶界碳化物的演變，有助於晶界強度的強化。對拉伸性能而言，拉伸強度提昇之原因是銖具有增加晶界細小碳化物數量及提昇 γ 基地強度的效果。而 γ 基地強度提昇的原因是銖具有固溶強化 γ 基地的效果。就潛變性能而言，與未添加銖之合金相較，含 3 wt.%銖之合金其潛變壽命延長約 2–3 倍。研究發現添加 1–3 wt.%銖時，會因：(1)立方體一次 γ′相(最佳化形貌 γ′相)數量的增加、(2)促進 γ′竹筏狀的發展及(3)增加 γ 基地強度等三項因素，降低合金之穩態潛變速率，延後潛變由穩態潛變階段進入加速(第三)潛變階段之時間。另晶界碳化物的細化及數量增加，會阻止裂縫沿著晶界成長，延長加速潛變階段的時間。綜上因素，促使含 1–3 wt.%銖之合金其潛變壽命延長。而添加 5 wt.%

過量的鉻，會因 P 相的形成造成拉伸及潛變性能的下降。

經由本論文之研究及探討證實，顯示添加 3 wt.%鉻是能維持 Mar-M247 細晶超合金顯微組織穩定和能提昇中高溫機械性能之最佳添加量。

Effects of Rhenium Addition on Microstructures and Mechanical Properties of Ni-Base Mar-M247 Superalloy

Student: Jian-Hong Liao **Advisor: Prof. Tzeng-Feng Liu**

Department of Materials Science and Engineering

National Chiao Tung University

Abstract

The effects of rhenium (Re) addition on microstructures and mechanical properties of Ni-base Mar-M247 superalloy were systematically investigated. The experimental results indicated that the grain size of the Mar-M247 superalloy with 0, 1, 3, and 5 wt.% Re content was 90, 70, 60, and 50 μm, respectively. The primary γ′ phase became finer and more cuboidal as Re content increased. The concentrations of Ta and Ti in strip-like MC carbides existing within the γ grains decreased as Re increased. The addition of 3 wt.% Re caused MC carbides within the grain to decompose into discontinuous $M_{23}C_6$ carbides and initiated the formation of a deleterious topological closed-packed (TCP) phase within the grain interior. The addition of 5 wt.% Re further promoted phase instabilities that led to the precipitation of large amounts of needle-like P phase within the grain interior, attributable to Re and W segregation.

The results of tensile tests carried out at temperatures ranging from room temperature to 760°C showed that the addition of 3 wt.% Re significantly improved the ultimate tensile strength and yield strength. Creep test performed

under the condition of 760°C/724MPa showed that the creep properties were primarily dominated by steady-state creep. The steady-state creep rate and creep life of alloy with 3 wt.% Re was respectively reduced by 31% and prolonged by 63%, as compared to those of the alloy without Re. Microhardness tests showed that addition of Re could enhance the strength of the γ/γ′ matrix, and the strongest γ/γ′ matrix could be obtained in the alloy with 3 wt.% of Re addition. The improvement in tensile and creep properties was associated with a decrease in grain size and an increase in the strength of γ/γ′ matrix caused by Re addition. However, by increasing the Re addition to 5 wt.%, degradations in both of the tensile and creep properties were obtained, presumably being due to the formation of needle-like P phase within the grain interior. Fracture analysis demonstrated that during tensile and creep tests, cracks initiated and propagated along grain boundary in 0–3 wt.% Re-containing alloys; however, in the alloy containing 5 wt.% Re, cracks initiated and propagated along both grain boundary and the P phase.

The results of 982°C tensile and 982°C/200MPa creep tests showed that both of the tensile properties and creep life increased with increasing the Re content up to a maximum at 3 wt.%. Quantitative statistical analysis showed a decrease in the size of grain boundary carbides and an increase in the number of grain boundary carbides as the Re content was increased. This grain boundary carbide evolution is conducive to the promotion of grain boundary strength. The tensile strength increased with increasing the number of fine grain boundary carbides and the strength of γ matrix. The improvement of the γ matrix strength was attributed to the solution strengthening effect resulted from the Re addition. The creep life of the alloy with 3 wt.% Re was extended by 2–3 times more than that of the Re-free alloy. The addition of 1–3 wt.% Re reduced steady-state creep

rates and postponed the onset of the acceleration stage in three ways: (1) by increasing the amount of primary cuboidal γ′ phase; (2) by increasing the development of γ′ raft; and (3) by increasing the strength of γ matrix. An increase in the duration to the accelerated creep stage was caused by both carbide refinement and an increase in the number of grain boundary carbides prevented cracks from propagating along the grain boundary. The above mentioned factors resulted in a prolongation of creep life. However, addition of excessive amounts of Re, such as 5 wt.% Re, causes deterioration of the tensile and creep properties due to the formation of P phase.

Consequently, the present study has critically identified that 3 wt.% of Re addition is the optimum concentration for obtaining fine-grain Mar-M247 superalloy with superior microstructural stability and much enhanced mechanical properties at moderate and elevated temperatures.

致謝

本論文承蒙劉增豐教授及朝春光教授多年來悉心的指導，使學生的研究實驗能夠順利且完成此論文，並感謝老師多年來的諄諄教誨，使我在學識上及待人處事上皆能有所精進，學生在此致上最誠摯的感謝。感謝賀俊教授、吳錫侃教授、莊振益教授等口試委員悉心指正，促使本論文更臻完整，在此並致謝忱。

感謝中科院薄慧雲組長的支持、鼓勵及照顧，讓我在工作百忙之中，有機會返回校園繼續深造，並在這段時間對我論文的指導，工作及生活上的關懷，在此要特別向薄組長您致上十二萬分的謝意。感謝在中科院共事的同事們，在我求學期間，都能體諒我在職進修的辛勞，不僅在實驗及工作上的協助，並在生活上時時刻刻的關心我，尤其是小組長魏肇男博士在我實驗及撰寫論文期間對我的指導及研究心得分享，雄哥陳俊雄先生及劉明浩領班等人在真空澆鑄上的幫助，並肩作戰的好伙伴毅龍分擔了我工作上不少的重擔，王承順博士在 TEM 實驗上的協助，倪國裕博士的英文撰寫指導，許淑華及朱黎明小姐在行政工作上的幫助，梁仕昌、游智惟、彭煥之先生及林佳詩、吳曉旻小姐的陪伴及關懷，讓我的生活增加不少的趣味。由於你們的協助及鼓勵，讓我得以順利取得學位。

感謝加測組同仁在實驗分析上的鼎力協助，提供實驗所需之儀器及設備資源，使得本論文得以順利完成，在此衷心向楊思誠副組長、蔡國棟博士、黃玉寶小組長、翁得恩先生、翁仁斌先生、陳錦國先生及范德鈞先生

等加測組全體同仁，一併致上衷心的謝意。

感謝實驗室楊秘書、志龍學長、柏至及永昌等學弟們及系辦余小姐在口試期間的協助，讓口試得以順利舉行，在此向你們說聲：「謝謝!」，祝福各位也都能早日順利完成學業。

感謝最疼愛我的母親與家人自始至終一直對我關心及鼓勵，給我充分的時間及精神上的支持，讓我能為自己築夢，並完成夢想，有了你們的愛，即使我再疲憊、失落、獨單，仍有堅毅的信心能堅持到最後，順利地完成學業，對此我內心有無限的感激。

最後，感謝主的恩典，在我身上一再印證給我的愛是何等的豐盛，因你的愛我得以站立的穩，願這一切的榮耀都歸於天上的父神。

Contents

List of Tables

List of Figures

Chapter 1.

General Introduction

General Introduction

A superalloy, usually based on group VIIIA elements, is an alloy developed for moderate and elevated temperature services, where relatively severe mechanical stressing is encountered and high surface stability is frequently required [1]. Superalloys are divided into three classes; nickel-base superalloys, cobalt-base superalloys, and iron-base superalloys [1]. These alloys always contain substantial alloying additions in solid solution to provide strength, creep resistance, or resistance to surface degradation [2]. After 1930s, iron generally disappeared as a superalloy base in favor of nickel and cobalt since they stabilized the stronger face-centered-cubic (FCC) structure at high temperatures [3]. In addition, the nickel-base alloys contain elements that, after suitable heat treatment, result in the formation of small coherent particles of intermetallic compound γ′ phase [$Ni_3(Al,Ti)$] [2]. The major contribution to the strength of precipitation-hardening nickel-base superalloy is provided by γ′ phase [4]. Due to the strength of γ′ phase increases with increasing temperature, the strength of nickel-base superalloys is superior to that of cobalt- and iron-base superalloys at the moderate and elevated temperatures.

The major phases present in most nickel-base superalloys are as follows:

1. Gamma (γ phase): The continuous matrix is an FCC nickel-base austenitic phase that usually contains high percentages of solid-solution elements such as Co, Cr, Mo, and W [5].
2. Gamma Prime (γ′ phase): The primary strengthening phase in Ni-base superalloys is $Ni_3(Al,Ti)$. It is a coherently precipitating phase (i.e., the crystal planes of the precipitate are in registry with the γ matrix) with an $L1_2$ (ordered FCC) crystal structure. The close match lattice parameter between

γ′ phase and γ matrix (~0-1%) combined with the chemical compatibility allows the γ′ phase to precipitate homogeneously throughout the γ matrix with long-time stability [6]. More remarkably, the strength of γ′ phase increases with increasing temperature up to about 800°C [6-7].

3. Carbides: Carbon combines with reactive and refractory elements such as titanium, tantalum, and hafnium to form carbides (e.g., TiC, TaC, or HfC). During heat treatment or when in service, these carbides begin to decompose into $M_{23}C_6$ Carbides, which tend to form heterogeneously on the grain boundaries [8]. It is generally concluded that in polycrystalline superalloys, carbides are beneficial to increase rupture strength at high temperatures [9-11].
4. Topologically Close-Packed (TCP) Phases: These brittle and undesirable phases can be formed during heat treatment or when the alloys are in service at high temperatures. The cell structure of these phases has close-packed atoms in layers separated by relatively large interatomic distances. The layers of close packed atoms are displaced from one another by the larger atoms sandwiched in between, leading to development of a characteristic "topology." These compounds have been characterized as possessing a topologically close-packed (TCP) structure [12]. The crystal structures of various TCP phases are very different. For instance, the μ and R phases are rhombohedral, the P phase is orthorhombic, and the σ phase is tetragonal [13]. TCP phases usually form as plates (which appear as needles on a single-plane microstructure). The TCP phases are reported to result in significant decrease of ductility and strength due to the following two primary reasons. First, its brittle nature and needle-like morphology are the major sources for crack initiation and propagation leading to brittle failure.

Second, the formation of TCP phases consumes the content of the alloying elements needed for solution-strengthening, thus resulting in a weakened matrix [13-14].

The fine-grain microstructure of Ni-base superalloys provides advantages, such as refined grain, carbides, and precipitates. The fine-grain process was developed to improve the strength, creep and fatigue life of disc rotors, turbine blades, and integral wheels operating at intermediate temperatures (427–760°C) [15-17]. However, for higher-temperature performance, such as turbine blades, a coarser grain microstructure would be preferred [15]. In fact, the desired grain size for integral casting is difficult to achieve, which has limited the wide scale application of fine-grain superalloy casting. To overcome this issue, engineers are seeking for developing new superalloys capable of maintaining high-temperature strength by fine-grain casting. Due to superior alloy design and control of the microstructure of Mar-M247 superalloy, the fine-grain casting of this material has been applied at temperatures of up to 982°C [18]. This study proposes a modified alloy based on Mar-M247 superalloy to further improve the high-temperature strength in fine-grain casting.

Mar-M247 is a nickel-base superalloy comprising approximately 60% volume fraction of ordered $L1_2$ γ' precipitates in a disordered face-centered cubic γ matrix [11]. It has been developed for applications requiring high strength at elevated temperatures and has been widely employed in the fabrication of advanced turbine blades and rotating parts in the aerospace industry because of its excellent castability and high-temperature properties [11, 18]. Previous researches have shown that fine-grain microstructure improves strength of Mar-M247 superalloy at low-to-intermediate temperatures of up to about 815°C [11].

The strength of Ni-base superalloys at high temperatures is determined primarily by the characteristics of the γ′ precipitates [19-20]. In modern Ni-base single-crystal superalloys, the volume fraction of γ′ phase is limited to 70 % [19-20]. On the other hand, the grain boundary strengthening elements, such as C, B, and Zr, have made the incipient melting temperature of polycrystalline superalloys lower than that of single-crystal superalloys. To avoid incipient melting, the solution heat treatment temperature of fine-grain Mar-M247 superalloy is limited, preventing it from attaining a volume fraction of γ′ phase as high as that found in single-crystal superalloys. Solid solution strengthening of the γ matrix becomes an alternative solution to further improve the strength of this alloy.

Recently developed single-crystal superalloys contain high quantities of Re, which act as solid solution strengtheners to further improve the high-temperature capability [13, 21]. However, little research has been devoted to address the influence of Re addition on fine-grain Ni-base superalloys. In this study, we selected Re as the element to modify Mar-M247 superalloy; however, the introduction of this element leads the microstructure susceptible to the formation of deleterious TCP phases when exposed to elevated temperatures [13, 21-23]. Therefore, the addition of Re must be strictly controlled in the design of superalloys to avoid the formation of TCP phase.

This study focuses on the effects of 0–5wt.% Re addition on the microstructures and mechanical properties of fine-grain Mar-M247 superalloy at moderate and elevated temperatures.

Chapter 2.

Experimental Procedure

Experimental Procedure

In this study, 0, 1, 3, and 5 wt.% elemental Re were added to Mar-M247 superalloy and named as A(0Re), B(1Re), C(3Re), and D(5Re), respectively. Re was added to Mar-M247 ingot by melting in a vacuum furnace and then pouring into investment cluster molds, to obtain cast rods using the Microcast-X technique. Microcast-X, developed by Howmet Corporation, is a fine-grain technique with controlled low superheat [14, 17]. The temperature gradient in the Microcast-X process was reduced to limit grain growth. The pouring and mold temperatures were 1380°C and 1100°C, respectively. Table 2.1 gives the original alloy compositions used in this study. The chemistries of each alloy were determined using X-ray fluorescence except for the Re content, which was determined by inductive coupled plasma (ICP) chemical analysis. Hot-isostatic press (HIP) was utilized in this study to eliminate casting pore that was one possible factor influencing the results of tensile and creep tests. HIP and heat treatment conditions were conducted according to Ref. 11. HIP was executed at 1185°C under gaseous Ar at a pressure of 172.4MPa for 4h. Heat treatment of the solid solution was conducted at 1185°C for 2h in vacuum, followed by cooling in argon gas. Samples were subjected to aging heat treatment at 871°C for 20h in a vacuum and then cooled to room temperature (RT) in the furnace.

General metallographic samples were polished and etched using 10mL HNO_3 + 5mL HCl + 30 mL lactic acid. Grain size was measured by determining the mean linear intercept of the grains using optical microscope (OM). Scanning electron microscope (SEM) was adopted to characterize the microstructures. Energy dispersive spectroscope (EDS) was used to determine the composition of various phases. Transmission electron microscope (TEM) was used to determine

the crystal structure of carbide and the TCP phase. Twin jet electrolytic etching was employed in 90% CH_3COOH+10% $HClO_4$ solution to prepare TEM specimens. The distribution of elements was determined using electron probe microanalysis (EPMA) map. The differential thermal analysis (DTA) method was used to investigate the effect of Re on solidus and liquidus temperatures. All DTA tests were performed at a heating rate of 5°C/min. in argon gas using alumina crucibles. Quantitative statistical analyses of the grain boundary carbide, including particle size and linear density, were measured from more than 400 carbides using an artificial calculation method based on SEM images.

The Vickers hardness (Hv) was measured in the γ/γ′ matrix of the grain interiors using a 100g load. The heat-treated cast rods of each alloy were machined into standard test bars with a gauge diameter of 6.3mm and gauge length of 26mm. Tensile tests were performed using an Instron 1125 universal test machine with 0.2 mm/min. crosshead speed at RT, 427°C, 760°C, and 982°C in atmosphere. Creep tests were carried out using constant-load creep testing equipment at 760°C/724MPa and 982°C/200MPa in atmosphere. Four tests were conducted for each tensile and creep test. Fracture surfaces were characterized by SEM. Longitudinal section samples were metallographically prepared, as described above, and examined by SEM.

Table 2.1 Chemical compositions of superalloys investigated (wt.%).

alloy / element	A(0Re)	B(1Re)	C(3Re)	D(5Re)
Re	0	0.97	2.92	4.99
Cr	8.35	8.41	8.42	8.40
Co	10.10	9.98	9.99	10.00
Mo	0.69	0.69	0.69	0.70
W	9.91	10.02	10.02	10.03
Ta	3.05	2.99	3.01	2.99
Al	5.42	5.38	5.33	5.37
Ti	1.0	0.98	0.98	0.97
Hf	1.32	1.22	1.29	1.22
C	0.15	0.14	0.14	0.14
B	0.02	0.02	0.02	0.02
Zr	0.04	0.04	0.04	0.04
Ni	bal.	bal.	bal.	bal.

Chapter 3.

Effects of Rhenium on Microstructure and Phase Stability of MAR-M247 Ni-Base Fine-Grain Superalloy

Effects of Rhenium on Microstructure and Phase Stability of MAR-M247 Ni-Base Fine-Grain Superalloy

3-1 Introduction

Mar-M247 superalloy is a typical and well known nickel-base superalloy used in investment casting. Through its optimal alloy design and microstructure control, Mar-M247 superalloy has high strength and creep resistance at elevated temperatures. Basically, Mar-M247 superalloy consists of about 60% volume fraction of the γ′ phase in the γ matrix, which is a solid solution strengthened by cobalt, molybdenum, tungsten, and chromium. Carbides have grain boundary (GB) strengthening effects and also contribute to strength and ductility [9-10, 25-27]. The fine-grain microstructure is beneficial for the strength, creep and fatigue life of the superalloy at moderate temperatures (427–760°C). Thus, the fine grain process was developed for moderate temperature service [15, 24]. Microcast-X, developed by Howmet Corporation, is a fine-grain technique with controlled low superheat and a high heat extraction rate [11, 14, 28]. This process offers the potential for producing cast with a fine-grain size of 65–125μm [11, 28].

The strength of Ni-base superalloys is mainly determined by precipitates of the ordered intermetallic γ′ phase in the γ matrix. Most related studies have reported a significant increase in strength with increasing γ′ volume fraction and decreasing γ′ size [29]. However, in modern Ni-base superalloys, the γ′ phase is limited at 65–70% volume fraction for maximum precipitation hardening [19]. Adding solid solution elements, such as Re, W, Ta, and Mo, would further improve the strength of superalloys. On the other hand, the reliability of γ′ phase

for long-term exposures at elevated temperatures is another concern for superalloys, since the growth of γ′ phase significantly degrades creep strength. Hence, recent studies have concentrated on adding refractory and slowly diffusing metals, such as Re and Ta, into the superalloy to retard the growth of γ′ phase [30].

Previous studies have added 3 and 6 wt.% Re in second- and third-generation single crystal superalloys, respectively, to improve their high-temperature mechanical properties [31-32]. Re is known to have effects that prevent γ′ coarsening during thermal exposure and strengthen the γ matrix by a solid solution mechanism [30-35]. However, if the Re content is excessive, it tends to promote phase instabilities that lead to the formation of deleterious TCP phases, such as σ, P, μ, and R, during exposure to a high-temperature environment [13-14, 21, 30, 36]. TCP phases are typically characterized by close-packed layers of atoms forming "basket weave" sheets, which are often aligned with the octahedral planes in the FCC matrix [12, 21]. Table 3.1 summarizes the basic crystallography of common TCP phases [13, 36]. Therefore, during the superalloy design process, the Re concentration must be controlled to stabilize the microstructure. However, until now, few studies have reported the effects of adding Re to fine-grain Ni-base superalloys.

This study investigates Mar-M247 superalloy with 0, 1, 3, and 5 wt.% additions of Re. It focuses on the effects of Re on microstructure and phase stability to determine the maximum allowable Re additions for the Mar-M247 superalloy.

3-2 Results

3-2-1 Microstructures

Figure 3.1 displays the grain size of the four superalloys after heat treatment. The grain size and standard deviation of alloys are listed in Table 3.2. The average grain size of alloys A(0Re), B(1Re), C(3Re), and D(5Re) was 90, 70, 60, and 50 μm, respectively. Clearly, increasing the Re content reduced grain size.

Figure 3.2 and Table 3.3 show the microstructure and EDS analysis of the alloys, respectively. The microstructures of the original Mar-M247 superalloy (alloy A(0Re)) indicated that the main phases comprised (1) the γ matrix, (2) the reinforced γ′ phase, (3) the rosette eutectic structure γ-γ′, (4) strip-like MC carbides within the grain interior and (5) particle carbides at the grain boundary (Figure 3.2a). The MC carbides within the grain interior were 10~20 μm long. In addition, EDS analysis of MC carbides indicated that they were rich in Ta and Ti. On the other hand, the particle carbides existing at the grain boundary had a size of 0.5~1 μm, and EDS analysis indicated that they were rich in Cr and W. The particle-like carbide was identified as FCC $M_{23}C_6$ carbide with a lattice constant of 10.5 Å by TEM (Figure 3.3). For alloy B(1Re), the microstructure revealed similar characteristics to that of alloy A(0Re). The microstructure of alloy C(3Re) revealed that discontinuous carbides were formed within the grain interior. The discontinuous carbides, with individual size of 0.5~1 μm, contained high levels of Cr and W elements (Table 3.2) and lined up to form structures 10~20μm in length, as shown in Figure 3.2b. Figure 3.2c shows a short needle-like precipitate that formed on the discontinuous carbides in alloy C(3Re). EDS measurements indicated that the precipitate had high Re and W contents (Table 3.2). Therefore, it should be identified as a TCP phase by its needle-like shape

and high Re and W contents. In this research, few needle-like TCP phases were observed in alloy C(3Re). Figure 3.2d is a back-scattered electron (BSE) micrograph of alloy D(5Re). In this mode, phases that are typically enriched with regard to heavy elements, such as Re and W, are clearly distinguishable against a dark background consisting of the γ and γ′ phases. The needle-like TCP phases (bright) were observed on particle carbides or in the vicinity of particle carbides within the grain interior. The TCP phases were 10–20 μm long, and EDS measurements indicated that they had high Re and W contents (Table 3.2). The TCP was identified as P phase, with an orthorhombic structure and lattice constant a=0.901nm, b=1.689nm, and c=0.471nm, by TEM (Figure 3.4). The grain boundary carbides reveal bright contrast, suggesting that they also contained high levels of heavy elements, and EDS measurements indicated that they had high Re and W contents (Table 3.2). The morphologies of grain boundary carbides of various Re-containing superalloys were very similar.

Figure 3.5 shows the morphology of γ′ precipitates. Both the primary block γ′ and the secondary γ′ phases were distributed in the matrix of alloy A(0Re). However, primary block γ′, primary cube γ′**,** and secondary γ′ phases were observed in alloy C(3Re). Finally, alloy D(5Re) contained primary cube γ′ and the secondary γ′ phase. The size of primary block γ′, primary cube γ′, and secondary γ′ were about 0.8, 0.3, and 0.05 μm, respectively.

3-2-2 The distribution of elements

EPMA maps were obtained for the as-heated (after heat treatment) samples. In alloy A(0Re), the result indicated that the elements Ta, Ti, and Hf were partitioned heavily to the MC carbide, while W appeared to be uniformly distributed (Figure 3.6). In alloy D(5Re), the elements of Re and W partition

heavily to the P phase and grain boundary carbide, while Ta, Ti, and Hf exhibit a low degree of segregation to part of the grain boundary carbide (Figure. 3.7). The area of γ matrix reveals uniform but lower concentrations of Re and W distribution.

3-2-3 DTA results

Figure 3.8a plots the DTA curves of Re-free and Re-containing samples. All tests were performed on the as-heated sample. Each solidus temperature measurement was resolved by using the onset temperature for the endothermic liquidus peak. The corresponding liquidus temperature was resolved as the maximum endothermic peak value [37]. The solidus and liquidus temperatures are shown in Figure 3.8b. The DTA results reveal that the liquidus temperatures of alloys A(0Re), C(3Re), and D(5Re) were 1363°C, 1365°C, and 1367°C, respectively. On the other hand, the solidus temperatures of alloys A(0Re), C(3Re), and D(5Re) were 1324°C, 1329°C, and 1331°C, respectively. The DTA results indicated that the solidus and liquidus temperatures both increased with Re content.

3-3 Discussion

3-3-1 Effect of Re content on grain size

Studies have reported that adding the high melting temperature element Re to multicomponent Ni-base alloys can increase the melting temperature [33, 38]. In this study, similar results were obtained: adding Re increases the solidus and liquidus temperatures of the Mar-M247 superalloy. It has been shown that crystal growth is dependent on solid/liquid interface diffusion in the solidification of metal [39]. For the Microcast-X process, a lower superheat of melting alloy which has a shorter solidification time to allow atoms to leave the liquid and join the crystal, therefore limits the grain growth. Thus, under some pouring temperatures, a higher melting temperature alloy with the lower superheat of the melting alloy limits the grain growth and yields a finer-grained microstructure.

3-3-2 Effect of Re content on γ′ phase

This study demonstrates that adding Re can prevent the primary cube γ′ phase from coarsening to the primary block γ′ phase. The γ′ coarsening is mainly controlled by the diffusion of γ′ formation elements, such as Al and Ti, to the γ′ phase [34, 40-41]. Previous studies have shown that Re inter-diffuses slowly in Ni. Atom probe investigations have shown pileup of Re solute atoms in the γ matrix ahead of the growing γ′ phase [33-34, 41-42]. Thus, the added Re that segregates at the γ/γ′ interface will reduce the growth rate of the γ′ phase by inhibiting the diffusion of Al and Ti to the γ′ phase. Therefore, the primary γ′ phase becomes finer as the Re content increases. A spherical γ′ phase was observed with a near-zero γ/γ′ lattice misfit, whereas misfit increased the

tendency for formation of γ′ phase with a cuboidal shape [43]. Re partitions in the γ matrix and causes high lattice misfit by its large atomic radius [33, 42]. Thus, the shape of primary γ′ phases were translated from block (near spherical) to cubical as more Re was added.

3-3-3 Effect of Re content on carbides and TCP phase

The compositions of strip-like MC carbide within the grain interior of alloy A(0Re) were mainly TaC and TiC. Ta and Ti had been reported to strengthen binding forces to such an extent that they make MC carbide degrade very slowly during exposure to high temperatures. Therefore, HIP and solution treatment, which were executed at 1185°C, cannot cause stable TaC and TiC to degrade in alloy A(0Re). However, the concentration of Ta and Ti in MC carbide of the grain interior fell as more Re was added. MC carbides were replaced by discontinuous carbides in alloy C(3Re). In previous report, $M_{23}C_6$ carbide has moderate to high Cr content [9-10, 24]. The carbon content of the discontinuous carbide is close to the theoretical value of $M_{23}C_6$ (20.7 at.%) and has moderate Cr content. Therefore, the discontinuous carbide should be the $M_{23}C_6$ carbide. An earlier investigation showed that MC carbide degenerated to $M_{23}C_6$ carbide over 980°C [44]. The reaction can be expressed as:

$$MC + \gamma \rightarrow M_{23}C_6 + \gamma'$$

The HIP and solution heat treatment used herein were performed over 980°C. Moreover, the amount of stable TaC and TiC carbides decreased as Re increased; therefore, unstable strip-like MC carbide degraded to discontinuous $M_{23}C_6$ carbide in alloy C(3Re). To the authors' experiment, MC carbide degraded to discontinuous $M_{23}C_6$ during the HIP process in alloy C(3Re). This reaction has also been reported in another Re-containing fine-grain superalloy (CM-681LC)

[24].

Previous researches showed that TCP phases might form if the refractory element concentration was too high (over 17 wt.%) in the alloy [13, 30-35]. In this study, few needle-like TCP phases formed on the discontinuous $M_{23}C_6$ carbide in alloy C(3Re), indicating that the addition 3 wt.% Re caused the TCP formation elements, such as Re and W, to segregate to the discontinuous $M_{23}C_6$ carbide at the critical level. Previous studies have also shown that the σ phase is the first TCP phase formed, and it provides nucleation sites for the other TCP phases. The σ phase is not the most thermodynamically stable; depending on the alloy composition, other TCP phases are formed from it [13]. Due to the low diffusivities of Re and W in Ni at elevated temperatures, the residual segregation of high levels of Re and W tends to form the P phase [21]. Indeed, large amounts of P phases appeared in alloy D(5Re). The P phase contained a large amount of refractory metal elements, including Re, W, Hf, Ta, and Mo, the total amount of refractory elements is 29 at.%, as shown in Table 3.2. The segregation of excessive refractory metal elements, especially for Re and W, promotes the formation of the stable P phase rather than other types of TCP phases. This study has demonstrated that Re and W play a pivotal role in the mechanism of P phase formation in this alloy. This result is consistent with other studies of Re-containing superalloy; however, the formation of the P phase should be prevented. It is noticed that no needle-like TCP phase was observed at grain boundaries in alloy D(5Re), although the grain boundary carbide contained large amounts of refractory metal elements. A study has reported that Hf and B concentrated at grain boundaries can inhibit the formation of TCP phases [40], but the detailed mechanisms are still unclear. Thus, more studies should be performed to examine this phenomenon.

3-4 Conclusions

The effects of Re addition on the microstructure and phase stability of cast fine-grain Mar-M247 superalloy herein are summarized as follows:

1. The sizes of grains with 0, 1, 3, and 5 wt.% Re additions are 90, 70, 60, and 50 μm, respectively, indicating that Re addition reduces grain size.
2. The primary γ′ phase becomes finer and more cuboidal as Re content increases.
3. With 3 wt.% Re addition, strip-like MC carbides within the grain degenerate into discontinuous $M_{23}C_6$ carbides. Needle-like TCP phases are very rare within the grain interior; therefore, 3 wt.% Re is critical to initiate the formation of the TCP phase.
4. With 5 wt.% Re addition, EPMA and EDS analysis revealed that the Re and W concentrated at the P phase and grain boundary carbide. The segregation of Re and W caused phase instabilities that led needle–like P phase to form within the grain interior, but no needle–like TCP phase formed at the grain boundary.

Table 3.1 Crystallography of the TCP phases

Phase	structure	Atoms per cell	Lattice constants (Å)		
			a	b	c
σ	tetragonal	30	8.80	-	4.54
P	orthorhombic	56	9.07	16.98	4.75
μ	rhombohedral	39	4.76	-	25.61
R	rhombohedral	159	10.90	-	19.54

Table 3.2 Grain size and standard deviation of alloys

Alloy	average (μm)	standard deviation
A(0Re)	90	20
B(1Re)	70	16
C(3Re)	60	13
D(5Re)	50	11

Table 3.3 Chemical compositions of various phases in these alloys given by EDS (at.%)

	MC carbide (Fig. 3.2a)	GB $M_{23}C_6$ carbide (Fig. 3.2a)	discontinuous carbide (Fig. 3.2b)	TCP phase (Fig. 3.2c)	P phase (Fig. 3.2d)	GB $M_{23}C_6$ carbide (Fig. 3.2d)
elements	alloy A(0Re)	alloy A(0Re)	alloy C(3Re)	alloy C(3Re)	alloy D(5Re)	alloy D(5Re)
C	36.9	15.2	19.9	19.0	6.7	16.7
Al	4.0	4.6	4.8	6.3	9.2	5.3
Hf	6.9	0.0	1.0	0.4	-	-
Ta	24.8	5.7	7.1	1.4	0.5	2.8
W	7.5	26.3	15.0	12.3	15.8	20.8
Re	-	-	6.3	8.8	11.2	12.8
Mo	1.1	2.1	-	-	1.5	1.2
Ti	12.6	1.2	2.8	0.7	1.2	-
Cr	1.4	9.2	8.1	10.5	10.7	11.9
Co	1.0	7.4	7.9	7.9	8.4	7.9
Ni	3.8	28.3	27.1	32.7	34.8	20.6

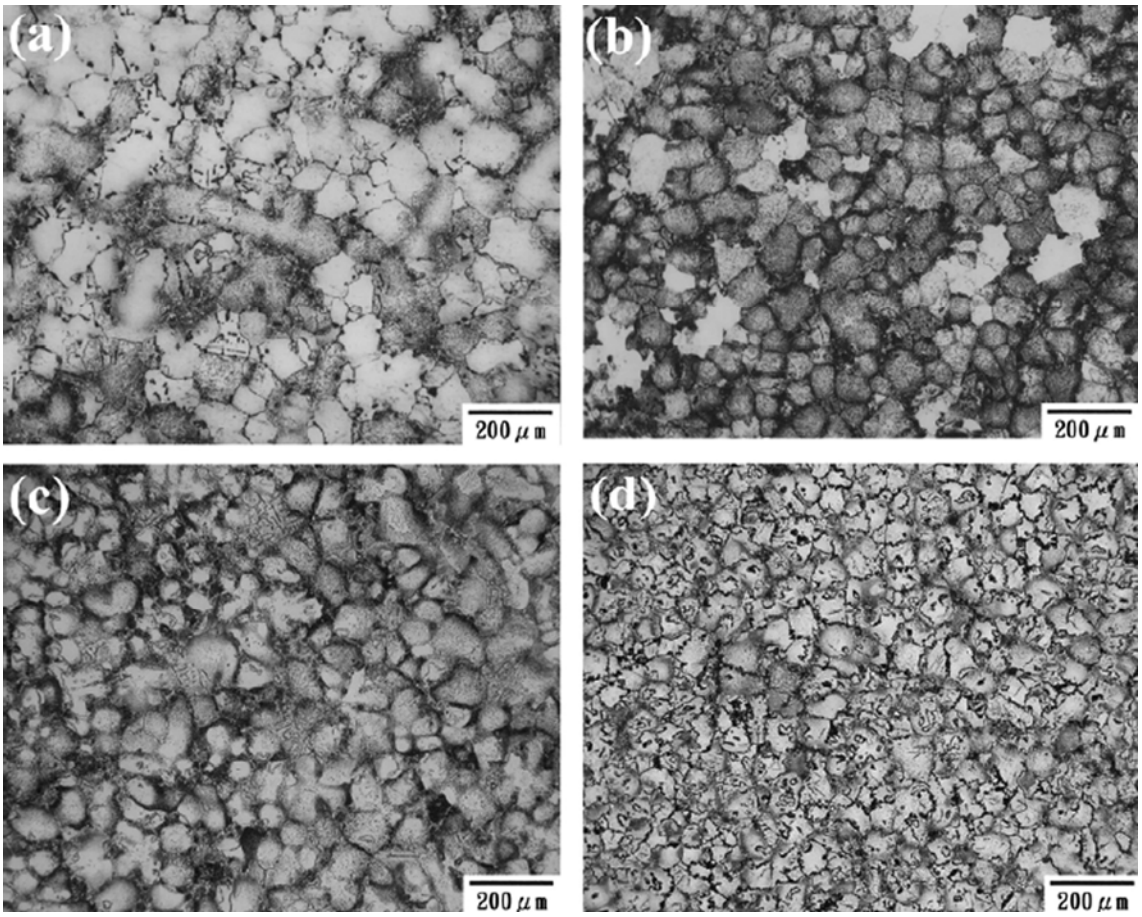

Figure 3.1 OM images of alloys (a) A(0Re), (b) B(1Re), (c) C(3Re), and (d) D(5Re) after heat treatment.

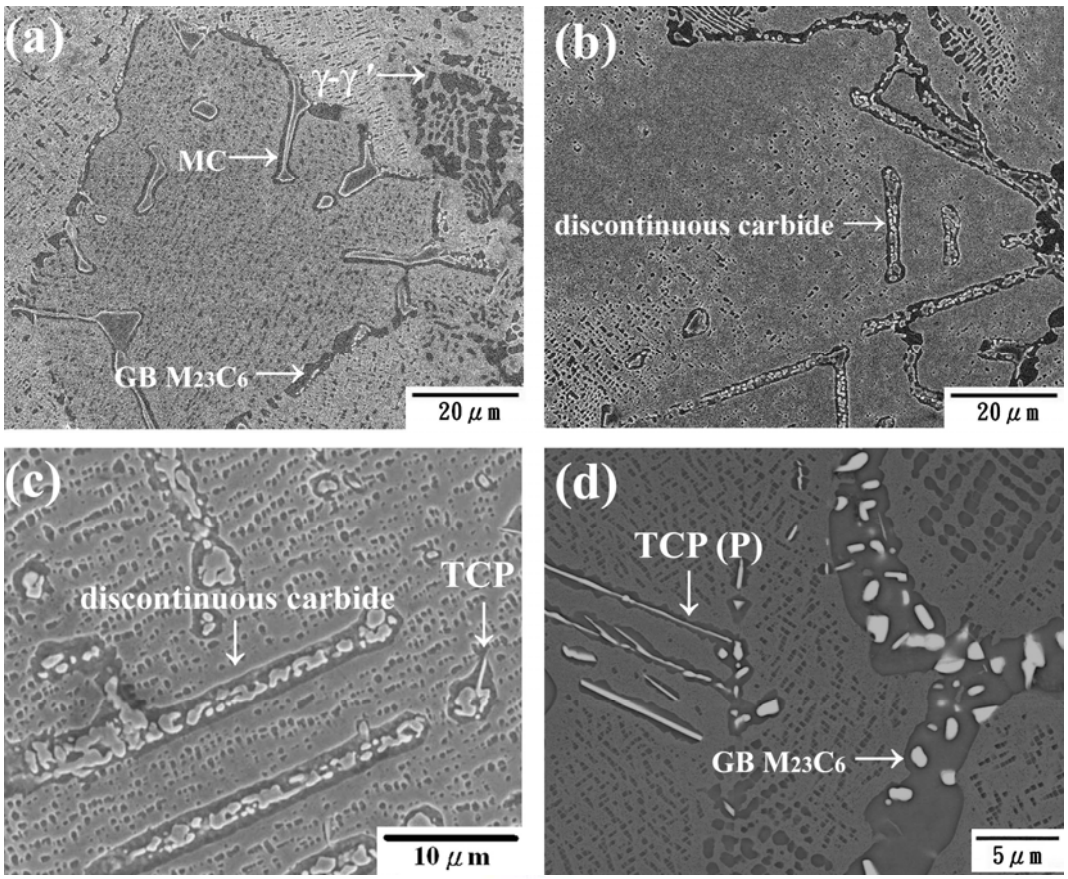

Figure 3.2 SEM microstructures of (a) alloy A(0Re), (b) alloy C(3Re), (c) TCP phase formation in alloy C(3Re), and (d) alloy D(5Re) (BSE images) after heat treatment.

(a)

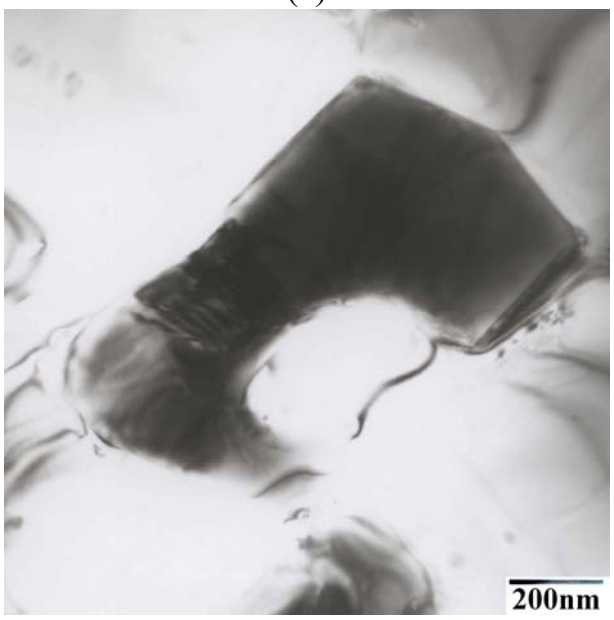

(b)

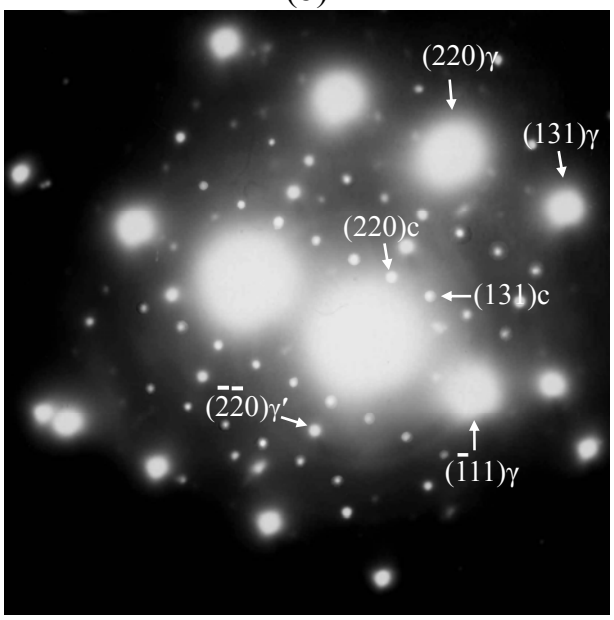

Figure 3.3 (a) TEM bright-field image of the $M_{23}C_6$ carbide and (b) selected area diffraction pattern (SADP) with $[1\ \bar{1}\ 2]$ zone in alloy A(0Re). Subscripts c, γ, and γ′ refer to the carbide, γ matrix, and γ′ phase, respectively.

(a)

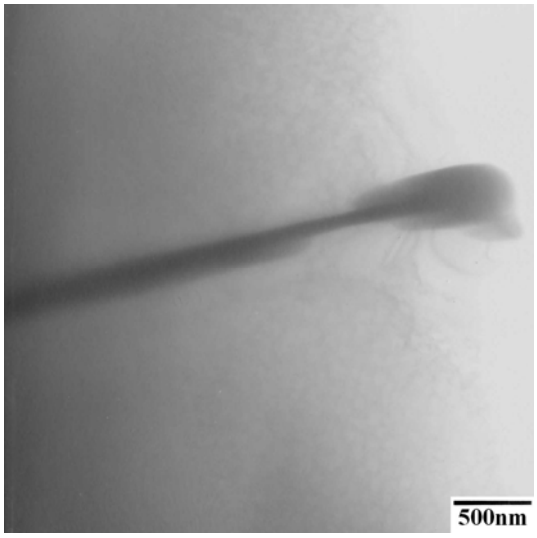

(b) (c)

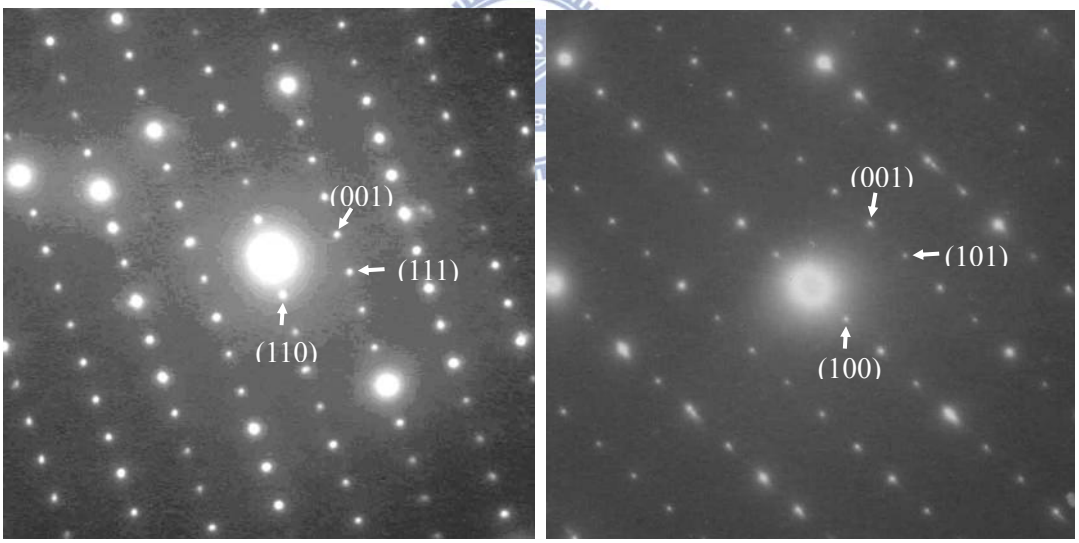

Figure 3.4 (a) TEM bright-field image of the P phase, (b) SADP with $[1\bar{1}0]$ zone, and (c) SADP with $[010]$ zone in alloy D(5Re).

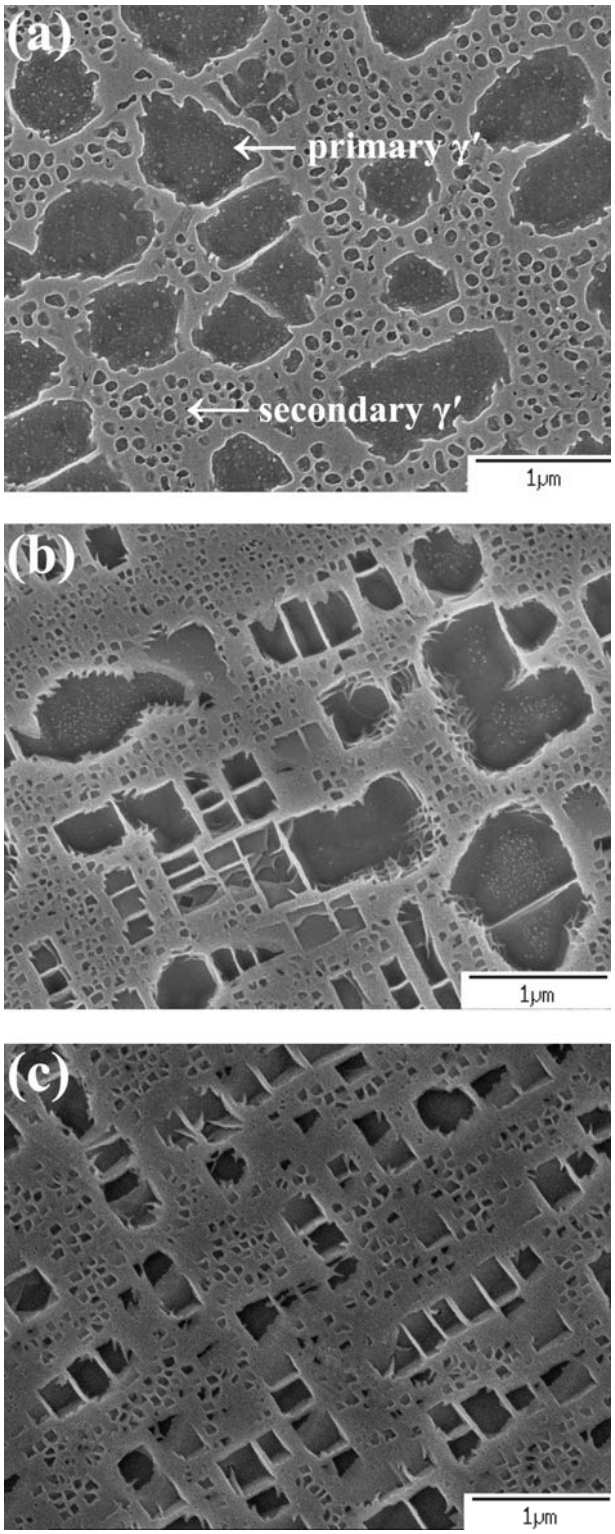

Figure 3.5 γ′ phase morphology of alloys (a) A(0Re), (b) C(3Re), and (c) D(5Re).

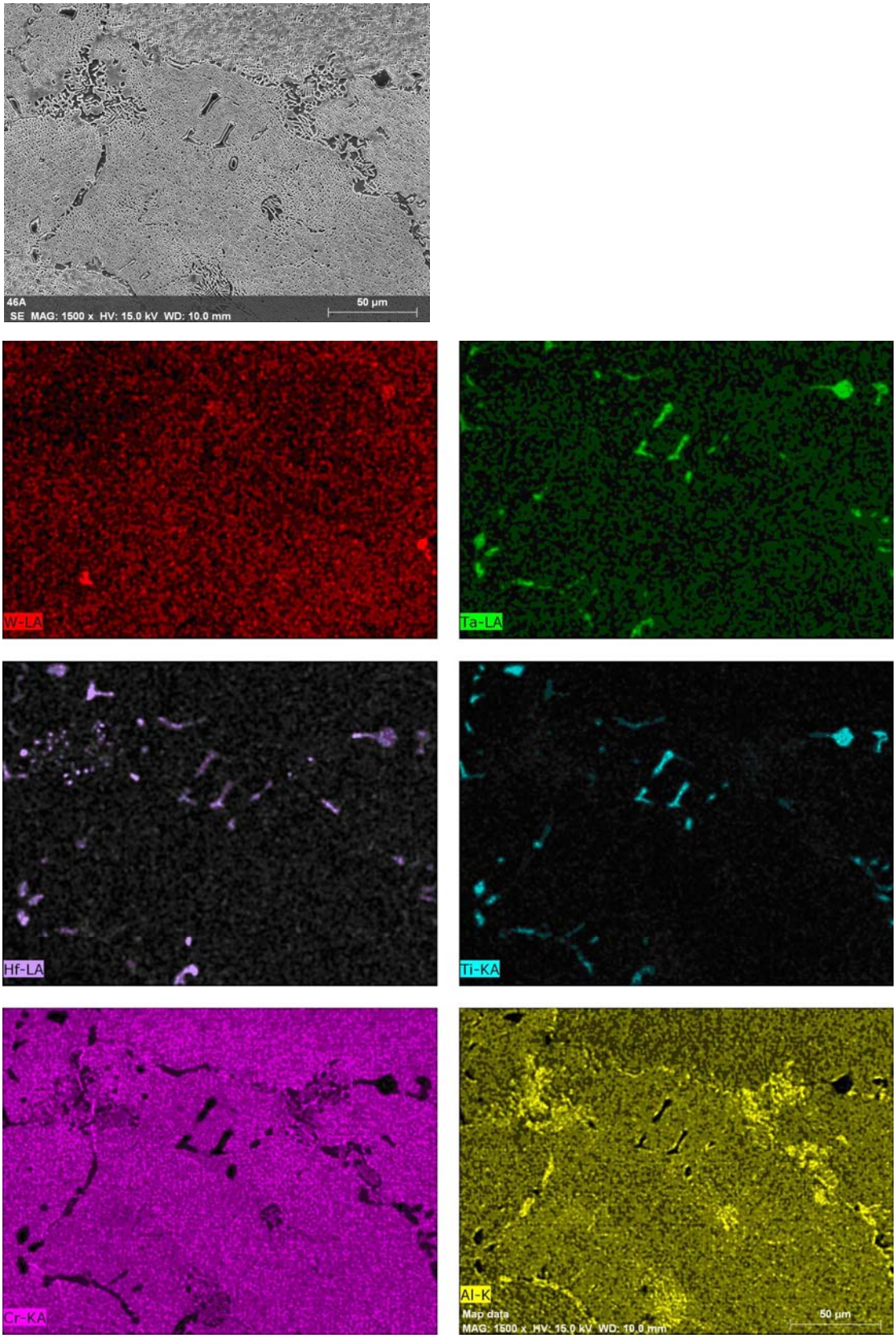

Figure 3.6 EPMA maps of alloy A(0Re)

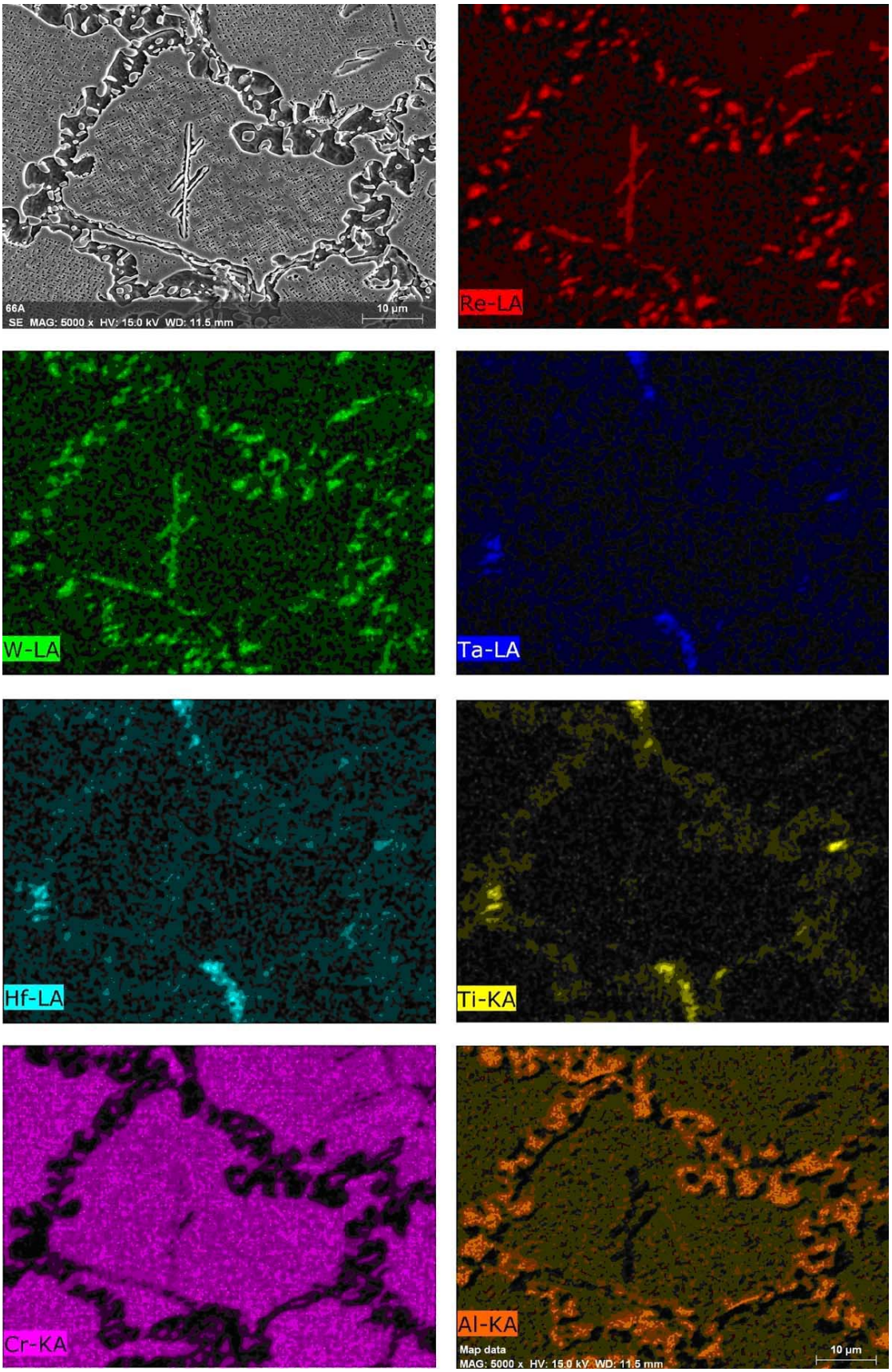

Figure 3.7 EPMA maps of alloy D(5Re)

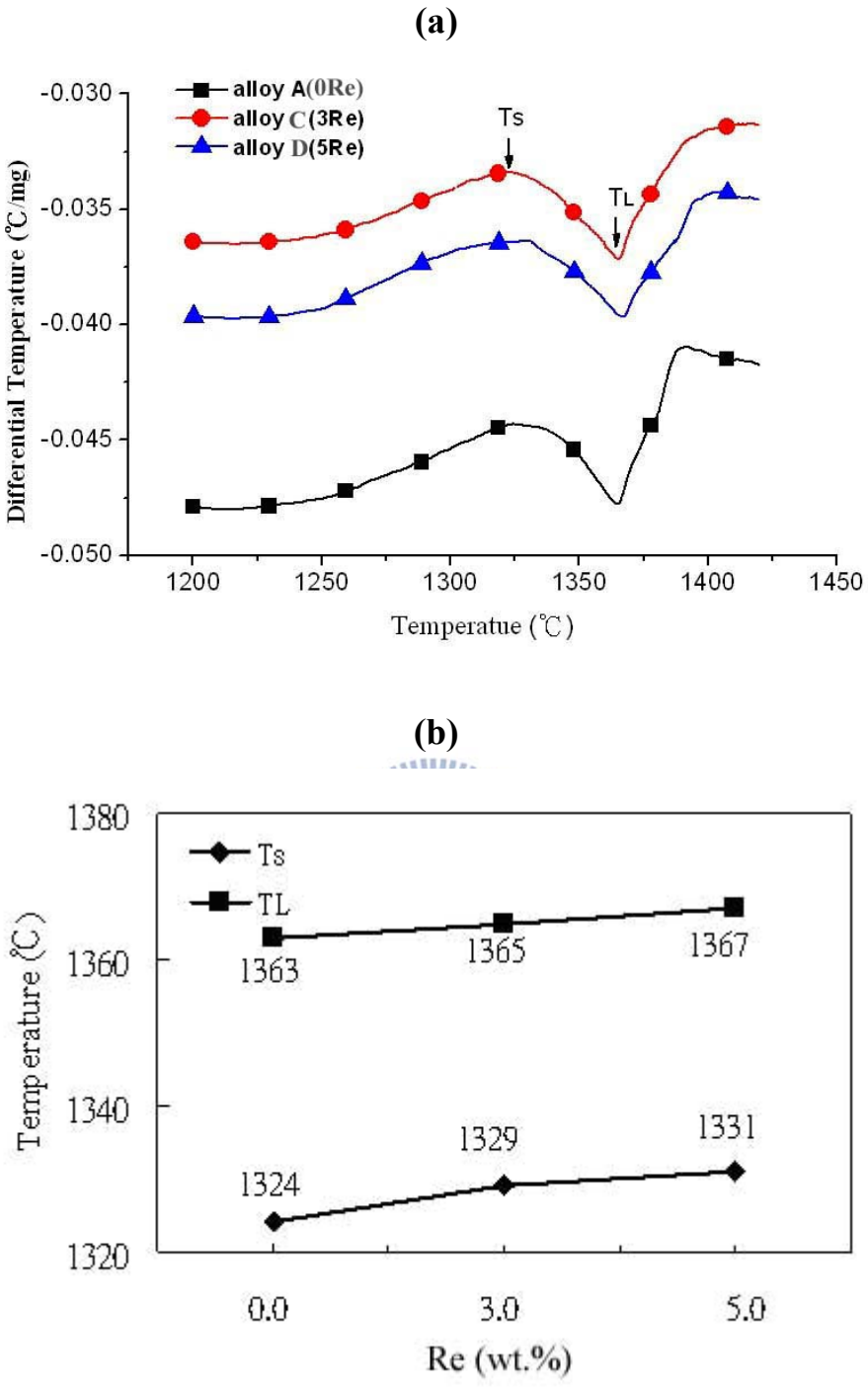

Figure 3.8 (a) DTA curves and (b) melting temperature (Ts: solidus temperature; T_L: liquidus temperature) of various Re-containing Mar-M247 superalloy.

Chapter 4.

Influence of Rhenium on the Mechanical Behavior and Fracture Mechanism of a Fine-Grain Superalloy at Intermediate Temperatures

Influence of Rhenium on the Mechanical Behavior and Fracture Mechanism of a Fine-Grain Superalloy at Intermediate Temperatures

4-1 Introduction

Developed by the Martin-Marietta Company in the 1970s, Mar-M247 superalloy is a typical polycrystalline Ni-base superalloy which is strengthened by γ′ phase precipitated in γ matrix [9, 11, 25]. Its optimal alloy design and microstructural control give Mar-M247 superalloy high strength for applications at elevated temperatures up to 1034°C [11]. This alloy has been widely employed in fabricating advanced turbine blades and rotating parts in the aerospace industry because of its excellent castability and high temperature properties [9, 11, 25-26]. Basically, Mar-M247 superalloy consists of about 60% volume fraction of the γ′ phase in the γ matrix, which is a solid solution strengthened by cobalt, molybdenum, tungsten and chromium [9, 11, 25-26]. Carbon is employed to enhance the grain boundary (GB) strength in this conventional polycrystalline superalloy [9, 11, 25-26]. Because the fine-grain microstructure has advantages such as refined grains, carbides and precipitates, the fine-grain process was developed to improve the strength, creep and fatigue life of disc rotors, turbine blades and integral wheels working at intermediate temperature (427~760°C) [15, 45 -46].

The strength of Ni-base superalloys is mainly determined by precipitates of the ordered intermetallic Ni_3(Al, Ti)-type γ′ phase in the face-centered cubic (FCC) γ matrix [47]. In modern Ni-base superalloys, the γ′ phase is limited to a 65–70% volume fraction for maximum hardening of precipitation [19-20].

Further improvement in the strength can be achieved through solid solution hardening of the γ matrix, e.g., by adding refractory elements, such as Re, W, and Ta [19]. The main advance in this field was the introduction of Re as a new alloying element, leading to the development of so called second generation (3 wt.% Re) and third generation (6 wt.% Re) single crystal superalloys [30-32]. Single crystal superalloys offer improved tensile and creep properties at high temperature (above 950°C) [20, 30-32]. Re is known to have beneficial effects in preventing γ′ coarsening during thermal exposure. It also strengthens the γ matrix with a solid solution [13-14, 30, 32-35]. However, if the Re content is excessive, it tends to promote microstructural instability and form deleterious topological closed-packed (TCP) phases during exposure to elevated temperatures [21, 36]. The crystal structures of the various TCP phases are very different. For instance, the μ and R phases are rhombohedral, the P phase is orthorhombic, and the σ phase is tetragonal [13]. A number of observations show that the brittle TCP phase could initiate and propagate cracks, significantly decreasing the tensile, creep, and ductility properties [22-23]. Therefore, during superalloy design, addition of Re must be controlled, to prevent formation of TCP phase. Most studies to date have focused on behavior of single crystal superalloys containing Re at high temperature. There appears to be a lack of research examining the influence of adding Re to fine-grain Ni-base superalloys, or its intermediate temperature performance.

This study investigates Mar-M247 superalloy with 0, 1, 3, and 5 wt.% additions of Re, focusing on the mechanical behavior and fracture mechanism of alloy at intermediate temperatures. This study determined the maximum allowable addition of Re to the Mar-M247 superalloy, to promote the tensile and creep properties.

4-2 Results

4-2-1 Microstructures

Figure 3.1 shows the grain size of four superalloys after heat treatment. The average grain size of alloys A(0Re), B(1Re), C(3Re), and D(5Re) was 90, 70, 60, and 50 μm, respectively. Figure 4.1 shows the microstructure of these alloys. Basically, the microstructure of alloy A(0Re) was similar to that of alloys B(1Re) and C(3Re). The microstructures of the alloys A(0Re) and C(3Re) indicated that the main phases comprised: (1) the γ matrix; (2) the reinforced phase γ′; (3) strip-like and blocky carbides within the grain interior; (4) particle carbides at the grain boundary; and (5) rosette eutectic structure of γ-γ′. The alloy A(0Re) showed a typical aged treatment microstructure, which consisted of γ′ particles 0.8 ~μm in size homogeneously distributed throughout the bulk samples. Alloy D(5Re) exhibited the non-homogeneously distributed γ′ phase; the fine γ′ particles existed in the core of the grain, however, the larger, block shaped γ′ particles (1~4 μm in size) were situated in the region near partial grain boundary (Figure 4.1c). In addition, the needle-like P phase was observed within the grain interior in the alloy D(5Re), and EDS measurements (Figure 4.1d) indicated that this phase had a high content of Re and W. Figure 4.2 shows the highly magnified SEM morphology of γ′ precipitates in the grain core. The block γ′ phases were distributed in the matrix of the alloy A(0Re). Block γ′ and fine cube γ′ were observed in alloy C(3Re); alloy D(5Re) contained the fine cube γ′. The size of block γ′ and fine cube γ′ were about 0.8 and 0.3μm, respectively. Finally, it is emphasized that no casting pores were observed in any of the alloys.

4-2-2 Microhardness and tensile tests

Figure 4.3a shows a typical OM image of alloy A(0Re) with micro-indentations in the γ/γ′ matrix. To investigate the influence of Re addition to the γ/γ′ matrix, the indentations were made in the γ/γ′ matrix, where no carbide, γ-γ′ eutectic phase, and TCP phase exist. Microhardness values of various Re containing alloys are shown in Figure 4.3b. The hardness values are averaged for over 20 indents. The average Hv of alloys A(0Re), B(1Re), C(3Re), and D(5Re) was 440, 445, 464, and 454, respectively. The results showed that the alloy C(3Re) had the γ/γ′ matrix with the highest degree of hardness.

The tensile properties of Mar-M247 superalloy with various Re content, tested at room and intermediate temperatures, are shown in Figure 4.4. In the results for RT tests, the average ultimate tensile strength (UTS), 0.2% offset yield strength (YS), and elongation (El) of alloy A(0Re) were 1131MPa, 977MPa, and 5.4%, respectively. Alloy C(3Re) exhibited the highest UTS and YS, which were 1203 and 1062MPa, respectively. The UTS and YS of alloy C(3Re) were promoted by 6.4 and 8.7%, respectively, as compared to alloy A(0Re). On the other hand, the El was quite similar to that of alloy A(0Re). Conversely, the UTS, YS, and El of alloy D(5Re) had decreased to 1095MPa, 944MPa, and 2.2%, respectively. In the results at intermediate temperatures, the tensile properties exhibited a similar tendency to those at RT. Alloy C(3Re) exhibited the best UTS and YS, and an El similar to that of alloy A(0Re), and the alloy D(5Re) displayed the lowest tensile properties.

4-2-3 Creep tests

Figure 4.5 illustrates the typical creep strain curves of Mar-M247 superalloy with various Re content at 760°C/724MPa condition. The creep curves of various Re-containing alloys show the same tendency, with a short primary stage of creep followed by a steady-state stage leading to failure, without entering the accelerating stage. For all of the alloys, the steady-state creep initiated at nearly the same strain (1%). It is obvious that the steady-state creep behavior dominated the creep properties. The creep data are listed in Table 4.1. According to Engine Material Specification EMS-55447 [48], the creep life of the Mar-M247 superalloy must be longer than 23 hours and the El must exceed 2% at 760°C/724MPa. During service, turbine blades are usually strained below 1 or 2%, therefore the criterion of time to reach 1% ($t_{1\%}$) or 2% strain ($t_{2\%}$) was chosen as a main indication for creep strength [11, 33]. For the alloys A(0Re), B(1Re), C(3Re), and D(5Re), the creep life and El are all exceeded specifications. It is obvious that the alloy C(3Re) has the longest $t_{1\%}$, $t_{2\%}$, and creep life, of 20.6, 89.7, and 124h, respectively. In other words, the $t_{1\%}$, $t_{2\%}$, and creep life of alloy C(3Re) were improved by ~47, ~53, and ~63%, respectively, compared to alloy A(0Re). Furthermore, compared with alloy A(0Re), the period of steady-state creep and the creep rate were effectively prolonged by ~67% and decreased by ~31%, respectively. Alloy D(5Re) exhibited the highest steady-state creep rate, and the shortest period of steady-state creep and creep life.

4-2-4 Fractographic observation

To investigate the effect of Re addition on fracture behavior in tensile and creep tests, both the fracture surface and longitudinal section adjacent to the

fracture region were examined. Observation from the fracture surface of a RT tensile tested specimen of alloy C(3Re) (Figure 4.6a), shows that the crack occurred mainly along the grain boundary. Figure 4.6b shows identical evidence to that in Figure 4.6a.: a continuous carbide particle film is clearly seen at the crack position of the grain boundary, indicating a typical intergranular fracture. A similar fracture was shown in alloys A(0Re) and B(1Re)—a crack was observed along the grain boundary. For the alloy D(5Re) sample, however, the fractography results were quite different. Observation of the fracture surface of alloy D(5Re) showed the crack on the grain boundary, and a secondary crack was observed within the grain interior (Figure 4.7a). In the longitudinal section, a crack was observed on the grain boundary, and needle-like TCP phases existed within the grain interior (Figure 4.7b), very similar in size to the length of the secondary crack observed in Figure 4.7a. No other phases in the microstructure had similar dimensions. As shown in Figure 4.7c, the microcracks were visible in the high magnification SEM fractography. Obviously, rupture occurred because the cracks initiated and propagated along the TCP/γ interface or at the TCP phase. The TCP phase was identified as W and Re-rich P phase by SEM/EDS (Figure 4.7d). In intermediate temperature tensile tests, each alloy had the same fracture mode as in the RT tests.

In the 760°C/724MPa creep tests, the fracture surface of alloy C(3Re) showed that cracks occurs mainly along the grain boundary (Figure 4.8a). Figure 4.8b showed identical cracking along the grain boundary, indicating a typical intergranular fracture. A similar fracture mode was shown in the alloys A(0Re) and B(1Re). For the fracture surface of alloy D(5Re), the cracks were observed on the grain boundary, and secondary cracks were observed within the grain interior (Figure 4.9a). Similarly, in Figure 4.9b, the cracks were observed on the

grain boundary and along the TCP/γ interfaces. The dimensions of needle-like TCP phase were similar to those of the secondary crack observed in Figure 4.9a. The microcracks were observed at the needle-like TCP phase (Figure 4.9c), and the TCP phase was identified as W and Re-rich P phase by SEM/EDS (Figure 4.9d). Finally, no evidence showed that that directional coarsening of γ′, which is called rafting, took place during the creep test in any of the alloys.

4-3 Discussion

4-3-1 Effect of Re content on the microhardness and tensile properties

The microhardness test performed within the grain interiors indicated the strength of γ/γ′ matrix. Although microhardness test verified that Re addition change the strength of γ/γ′ matrix, it is hard to estimate the difference of the γ/γ′ matrix strength is affected by γ′ precipitate or γ matrix. Most studies reported that the large atomic radius of Re mainly partitioned to the γ matrix increase the γ/γ′ lattice misfit, and a large lattice misfit produced large random stresses in the γ matrix, improving the strength of γ matrix [20, 31]. Moreover, Mott concluded that solid solution hardening could be accounted for by internal strain generated by inserting solute atoms into an elastic matrix [49]. K. durst used nanoindenting atomic force microscope to test the hardness of γ and γ′ phases in Re-containing superalloys, supporting the view described above [31]. In that research, it was shown an increase in the hardness of the γ matrix resulting from a higher concentration of Re, and no significant difference in the hardness of the γ′ phase. Therefore, the improvement of the γ/γ′ matrix strength within the grain interior probably attributes to Re solute strengthening of the γ matrix. The microhardness test results showed that adding 3wt.% Re could maximize the strength of γ/γ′ matrix, and then decrease with an addition of 5wt.% Re addition. The drop in strength of the γ/γ′ matrix in alloy D(5Re), which was caused by formation of the TCP phase, resulted from a depletion in the surrounding γ matrix of Re and W that were solid solution strengthening elements.

Tensile tests showed that alloy C(3Re) exhibited the highest UTS and YS. In comparison with alloy A(0Re), alloy C(3Re) increased the UTS to 6.4, 6.9, and 7.2%, and YS to 8.7, 9.5, and 8.2% at RT, 427, and 760°C, respectively.

Conversely, alloy D(5Re) decreased both UTS and YS. On the other hand, the El was nearly constant (5.2~5.8%) in alloys A(0Re), B(1Re), and C(3Re) at various temperatures. It is obvious that adding 3 wt.% Re could not affect the ductility, compared to an alloy without Re. However, the El decreased when the Re level was increased to 5 wt.% at room and intermediate temperatures. The effects on the grain size, γ/γ′ matrix strength, and TCP phase on tensile properties are discussed as follow.

Generally, the strength of an alloy strongly depends on grain size. According to the Hall-Petch equation, strength is a function of the reciprocal of the square root of the grain size [50]. It is well known that the grain boundary acts as an obstacle to slip dislocations. Thus, the applied stress required to cause a slip to pass through the grain boundary increases with a decrease in grain size. In theory, if grain size is considered the only influence on strength, alloy D(5Re) should have the highest strength at RT and intermediate temperatures. In fact, the alloy C(3Re), rather than alloy D(5Re), showed the highest UTS and YS. The microhardness testing showed that alloy C(3Re) exhibited the highest strength of the γ/γ′ matrix representing the highest ability to impede dislocation to move in γ/γ′ matrix. Although, alloy D(5Re) revealed the second highest γ/γ′ strengthening in this study, it exhibited the worst tensile properties. There must be other factors causing the drop in strength of alloy D(5Re). The presence of TCP phases was reported to result in significantly decreased ductility and strength in two ways: First, its brittle, needle-shaped morphology is ideal for crack initiation and propagation, leading to brittle failure; and the formation of TCP phases decreases the solution strengthening metal content in the γ matrix [13-14, 40]. Fractographic analysis verified that microcracks existed in the P phases, indicating that the needle-liked P phases were associated with a local

stress concentration, which may potentially act as initiation sites for cracking. In addition, the W and Re-rich P phases decreased the strength of alloy, due to the removal of solid solution strengthening elements from the γ matrix. While the crack initiated on the P/γ interface, the γ/γ′ matrix did not have enough strength to resist crack propagation. Thus, cracks propagate easily along the P phases under stress. As mentioned above, grain refinement and improvement in the strength of the γ/γ′ matrix contributed to the improvement of UTS and YS of alloy C(3Re). The formation of the needle-shaped P phase appeared to be a major contributing factor in the deterioration of the tensile properties in alloy D(5Re).

4-3-2 Effect of Re content on the creep properties

It has been reported that a greater curve in grain boundary makes grain boundary more difficult to slide [51]. In addition, the finer grain makes cracks along the grain boundary that have longer cracking paths to crack, consequently, harder to rupture. Therefore, a finer grain size, with more curved grain boundary, is beneficial for the creep life and El. According to the creep deformation map of a Mar-M247 related superalloy (Mar-M200), the creep mechanism under the conditions of 760°C/724MPa was controlled by dislocation glide [52]; that is, the creep behavior was dominated by the interaction between dislocations and obstacles such as γ′ precipitates. Moreover, the mobility of dislocations in γ/γ′ matrix during the creep depends on the strength of the γ matrix and is related to γ′ strength, size, and spacing (the distance between the γ′ precipitates). Firstly, the Re addition increases the strength of the γ/γ′ matrix representing increase of the γ or γ′ strength to inhibit dislocation motion. Secondly, most studies show that a cuboidal γ′ with a size of ~0.1–0.5μm can efficiently impede dislocation motion, and consequently achieve the best creep strength [40, 53]. In this study,

the morphology of the γ′ phase translated from a coarse block shape (0.8μm in size) to fine cuboidal shape (0.3μm in size) as Re content increased from 0 to 5 wt.% is another factor to improve creep strength. Finally, Re addition can increase amounts of small particle of γ′ exist in the γ matrix, resulting in shorting of the γ′ spacing to hinder the dislocation movement.

As mentioned above, the alloy D(5Re) with the finest grain and γ′ size should show the best creep properties, however creep life is substantially prolonged in alloy C(3Re), rather than in alloy D(5Re). Fractographic observations showed that the cracks of alloys A(0Re), B(1Re), and C(3Re) were along the grain boundary; however, the fractographic observations show that, for alloy D(5Re), the cracks were along the grain boundary as well as along the P/γ interface—adding another source for carking. The needle-like TCP phase could act as a barrier for moving dislocations, leading to incoherence in the weak P/γ interface, thereby causing interfacial cracks [40]. Moreover, formation of the P phase consumed the Re and W solid solution strengthening elements, resulting in a decreased resistance to dislocation moving in the γ matrix. Thus, the P phase caused creep accelerates to failure, which could be verified by the highest steady-state creep rate in alloy D(5Re). In addition, SEM observation of alloy D(5Re) showed inhomogeneously distributed γ′ phase, with the large γ′ phases existing in the region near the grain boundary. To authors' experiment, this coarse γ′ phases appeared in as-cast state. Obviously, as Re additions are increased, complete homogenization of solidification becomes difficult. It also indicates that the solution heat treatment condition used in this study cannot solute the coarse γ′ phases. The increase of the local γ′ particle size is another factor damaging the creep strength. However, no crack occurred at the coarse γ′ phases. Therefore, the formation of needle-like P phase seemed to play the

major detrimentally affecting creep properties in alloy D(5Re). In summary, a decrease in grain and γ′ size and an increase in strength of the γ/γ′ matrix contributed to the improvement in creep strength. Conversely, the formation of needle-like P phase is detrimental to the creep properties.

4-4 Conclusions

The effects of Re addition on the mechanical behavior and fracture mechanism of a fine-grain superalloy at intermediate temperatures are summarized as follows:

1. Microhardness tests showed that addition of Re could promote the strength of the γ/γ′ matrix. In particular, adding the 3 wt.% Re to Mar-M247 superalloy produced the strongest γ/γ′ matrix.
2. Grain refinement and improvement of the γ/γ′ matrix strength contributed to the improvement of UTS and YS of alloy C(3Re). The decrease in tensile properties of alloy D(5Re) was caused by the formation of needle-like P phase.
3. The 760°C/724MPa creep tests showed that the steady-state creep behavior dominated creep properties. The steady-state creep rate and creep life of alloy C(3Re) was reduced by 31% and prolonged by 63%, respectively, compared to alloy A(0Re). The improvement in creep strength was associated with a decrease in grain and γ′ size and an increase in strength of the γ/γ′ matrix. The formation of needle-like P phase, which increases the creep rate, was the major detriment to the creep life of alloy D(5Re).
4. Cracks initiated and propagated along the grain boundary in alloys A(0Re), B(1Re), and C(3Re) in the tensile and creep tests. For alloy D(5Re), the cracks initiated and propagated along both the grain boundary and P/γ interface.

Table 4.1 Creep test results of Mar-M247 superalloy with various Re content under 760°C/724MPa.

alloy	Creep life (h)	El (%)	*$t_{1\%}$ (h)	*$t_{2\%}$ (h)	*Steady-state creep rate (s^{-1})	*Period of steady-state creep (h)
EMS-55447	＞23	＞2	-	-	-	-
A(0Re)	65~75.9	2.1~2.3	14.0	58.8	5.83×10^{-8}	61.9
B(1Re)	72.8~83.6	2.1~2.6	18.1	70.7	5.09×10^{-8}	65.5
C(3Re)	108~124.0	2.1~2.5	20.6	89.7	4.03×10^{-8}	103.4
D(5Re)	33~47.6	2.0~2.2	12.5	41.1	9.59×10^{-8}	35.1

* obtain from creep curves of figure 4.5.

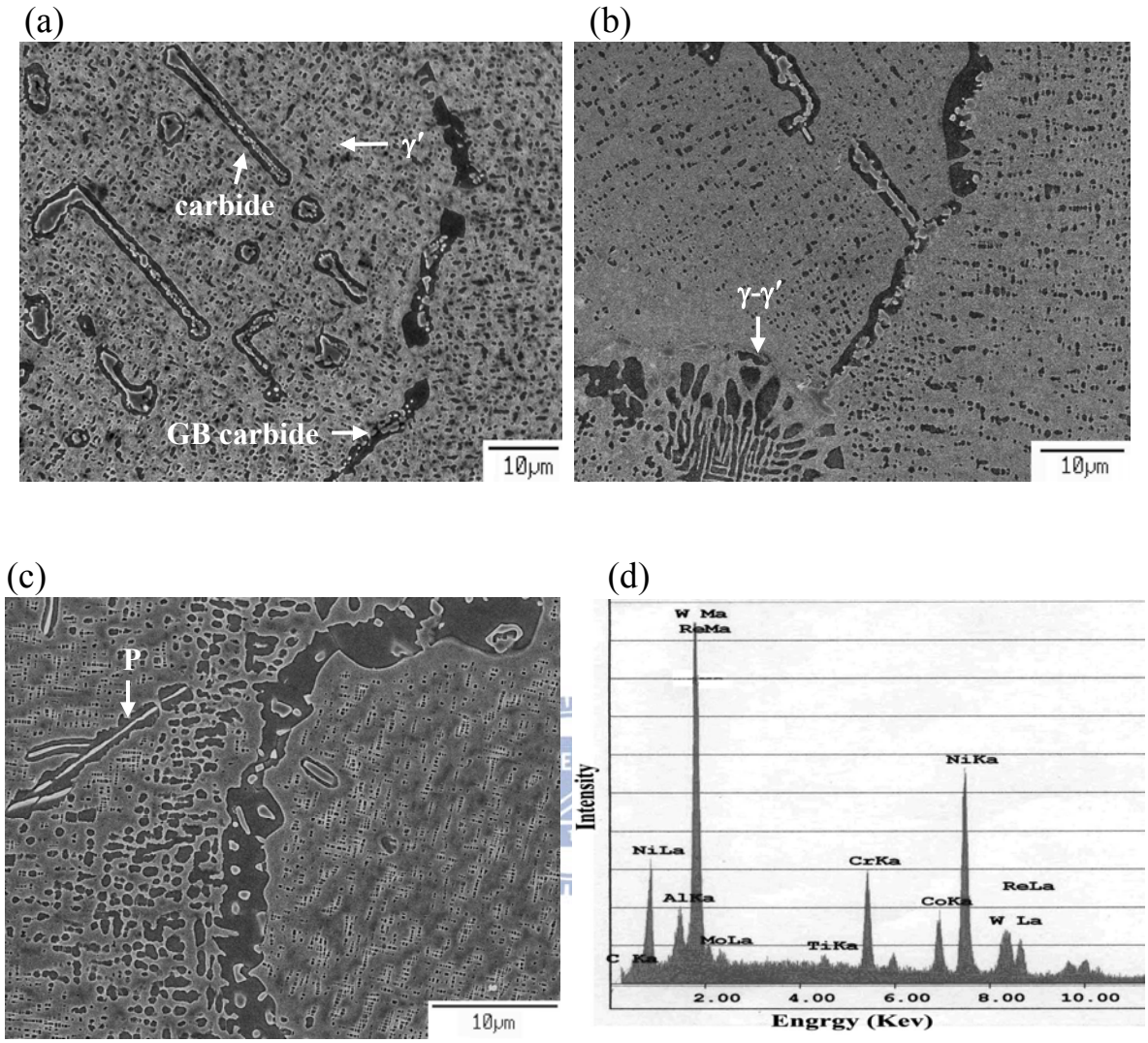

Figure 4.1 SEM microstructures of alloys (a) A(0Re), (b) C(3Re), and (c) D(5Re) after heat treatment. (d) EDS spectrum of TCP phase in alloy D(5Re).

(a)

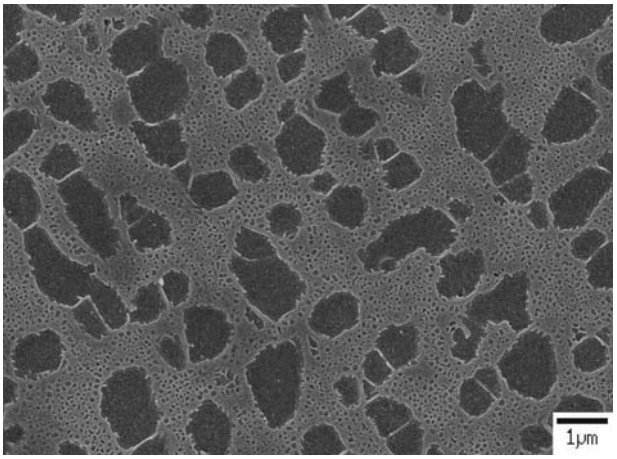

(b)

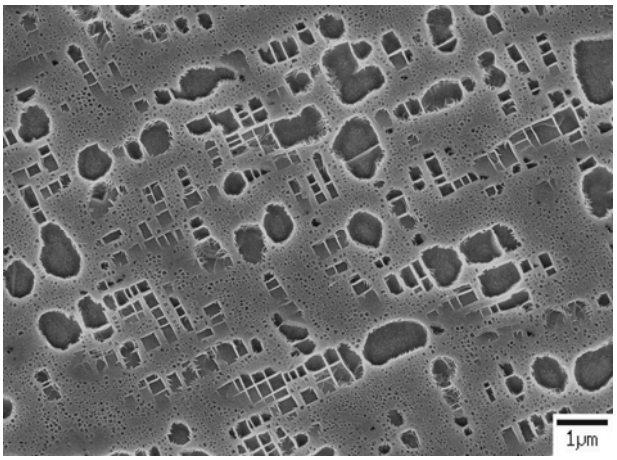

(c)

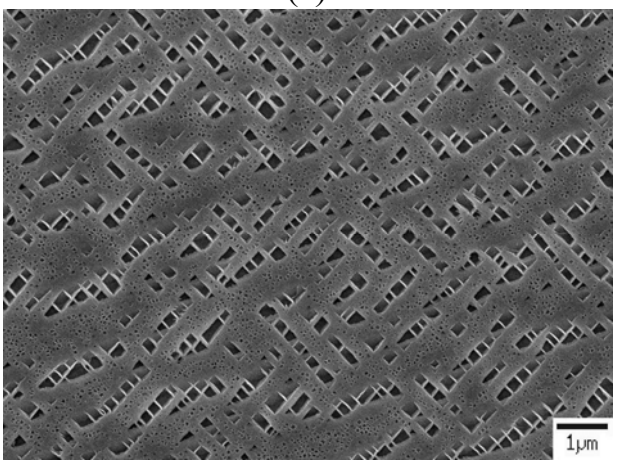

Figure 4.2 γ′ phase morphology in grain core after heat treatment. Alloys (a) A(0Re), (b) C(3Re), and (c) D(5Re).

(a)

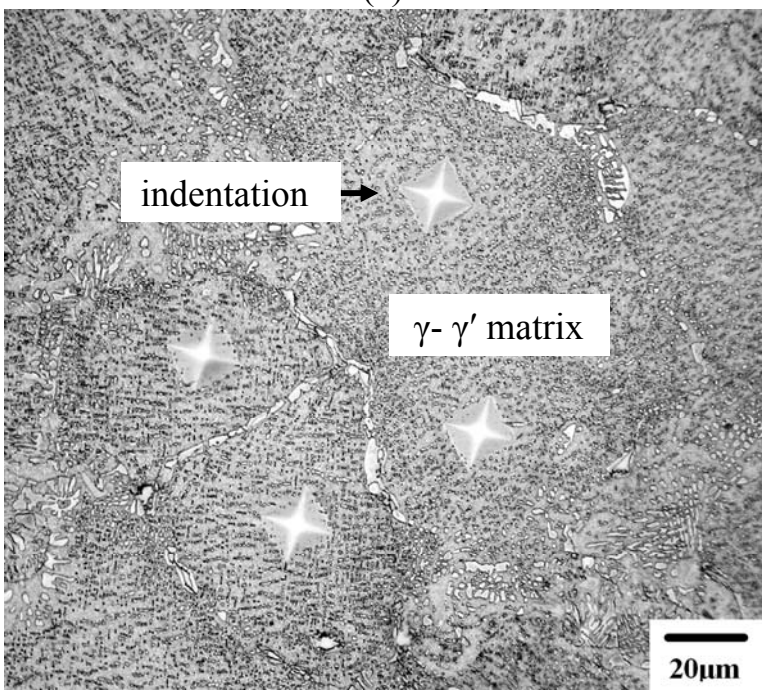

(b)

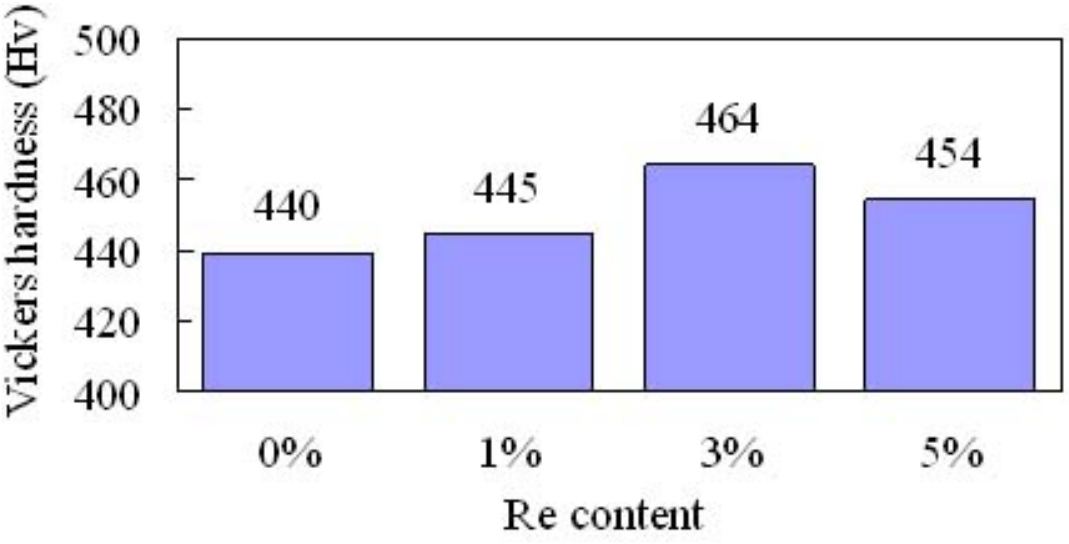

Figure 4.3 (a) OM image of alloy A(0Re) with micro-indentations in the γ/γ′ matrix and (b) Micro-Vickers hardness.

(a)

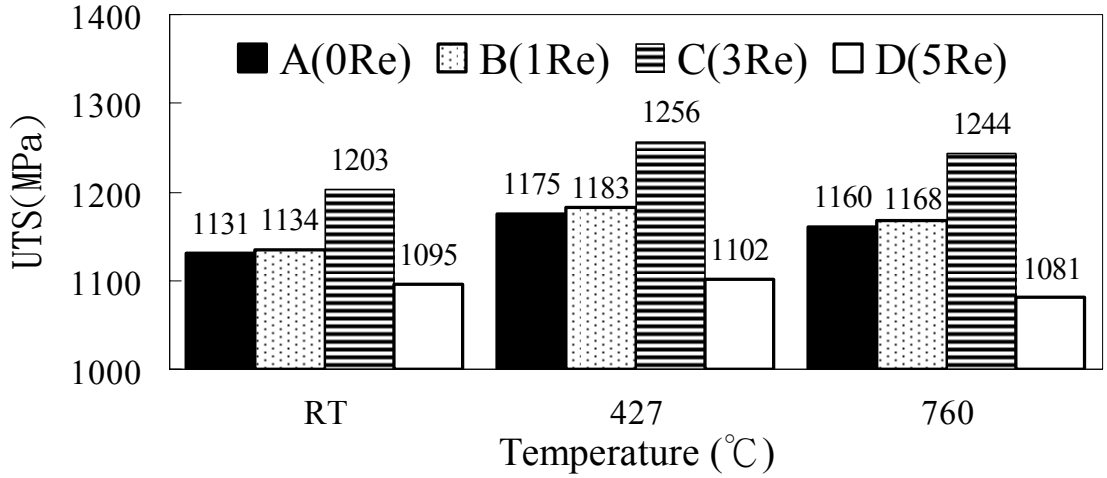

(b)

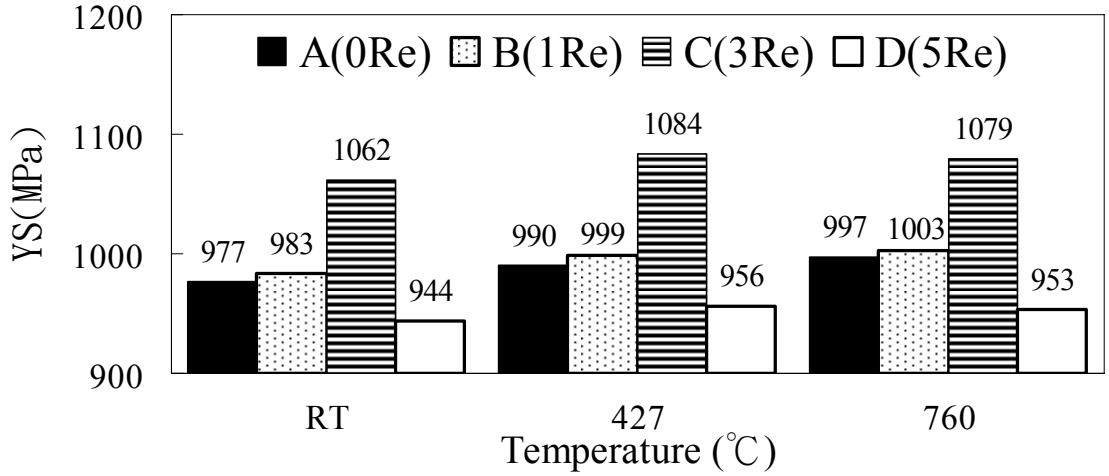

(c)

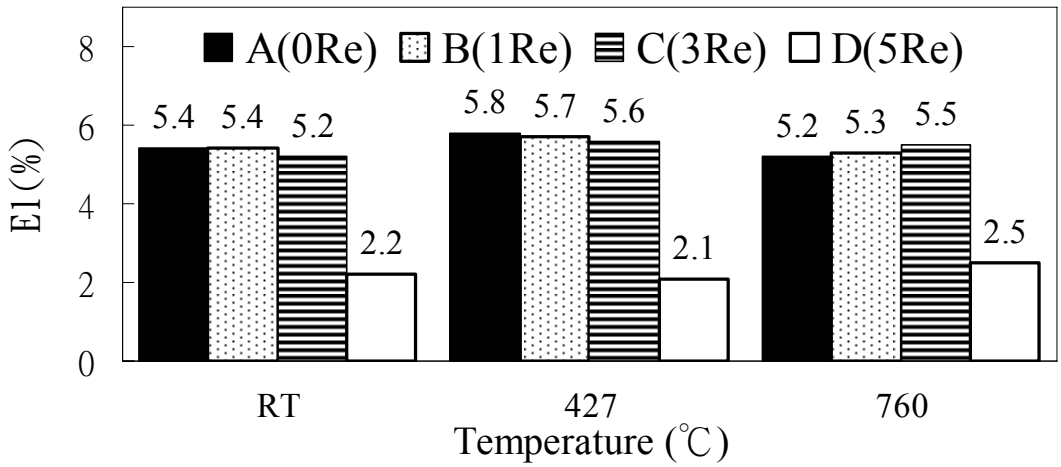

Figure 4.4 Tensile properties of Mar-M247 superalloy with various Re content tested at various temperatures. (a) UTS, (b) 0.2% offset YS, and (c) El (average value).

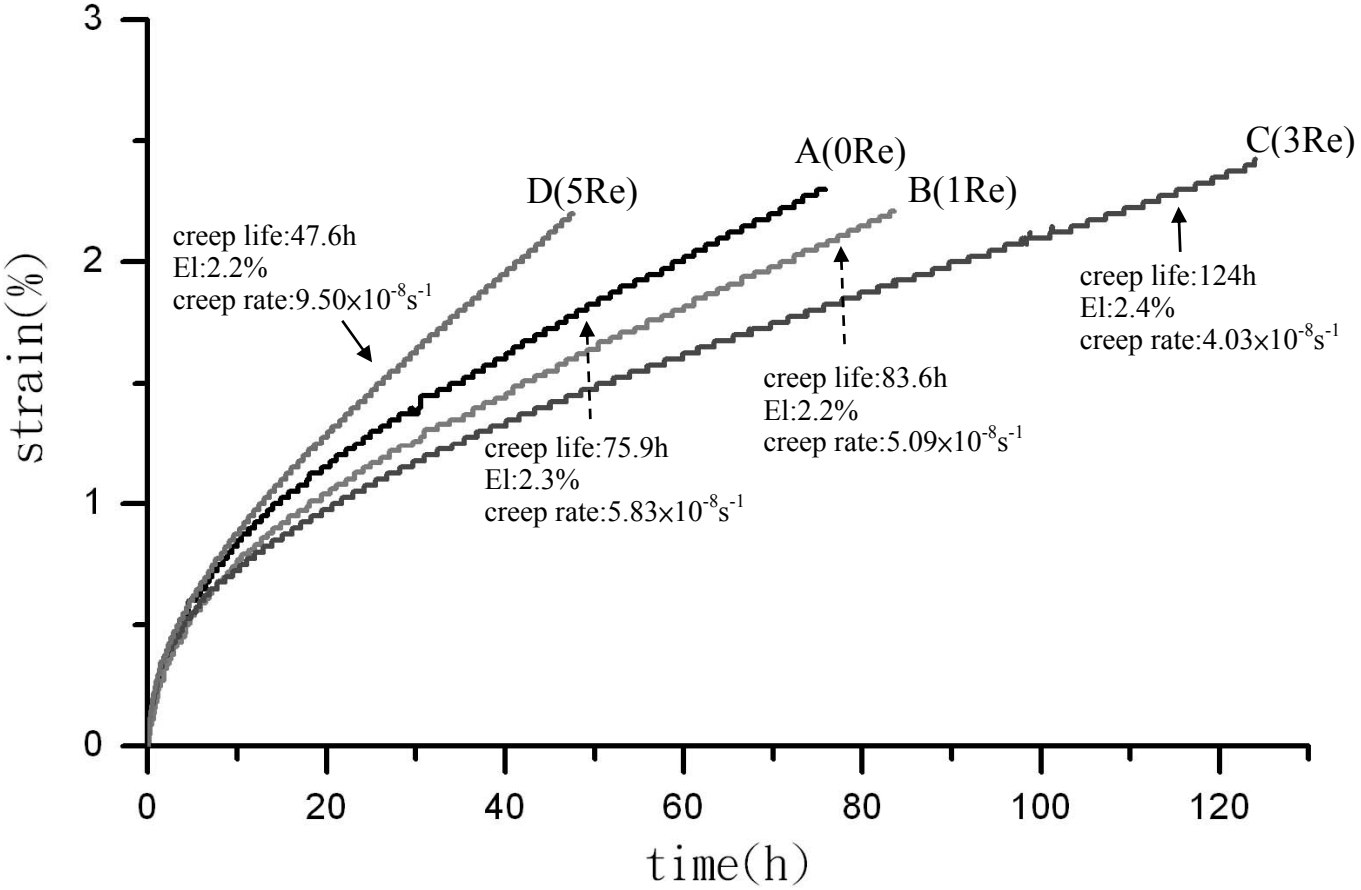

Figure 4.5 Creep curves of Mar-M247 superalloy with various Re content tested under 760°C/724MPa.

(a)

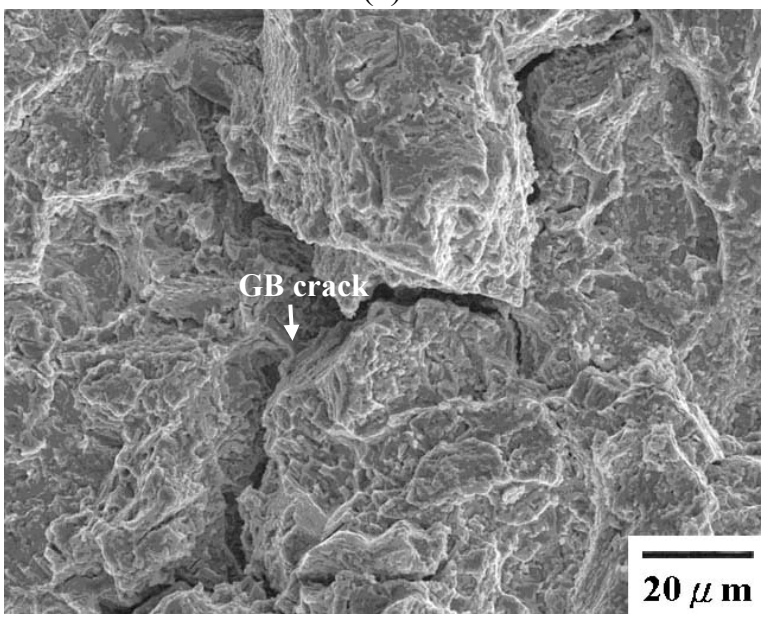

(b)

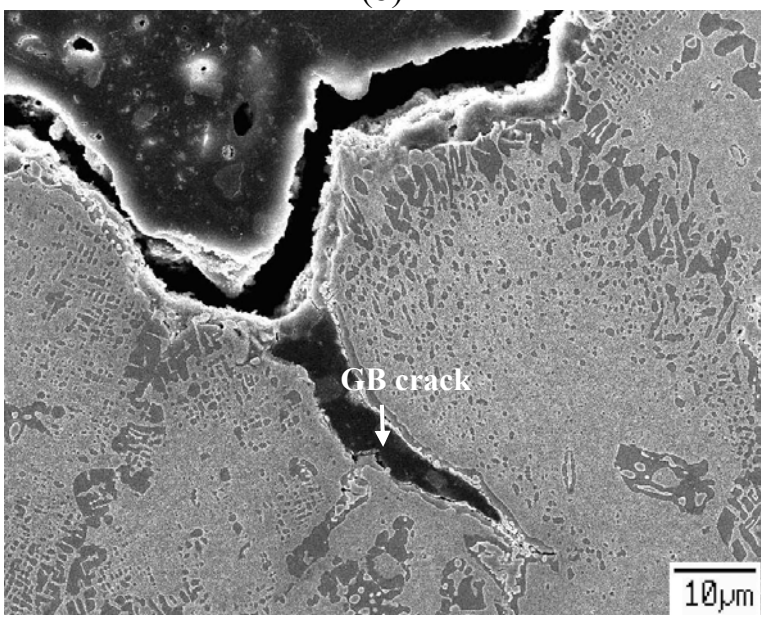

Figure 4.6 Fractographs of the alloy C(3Re) after RT tensile test. (a) Fracture surface and (b) longitudinal section.

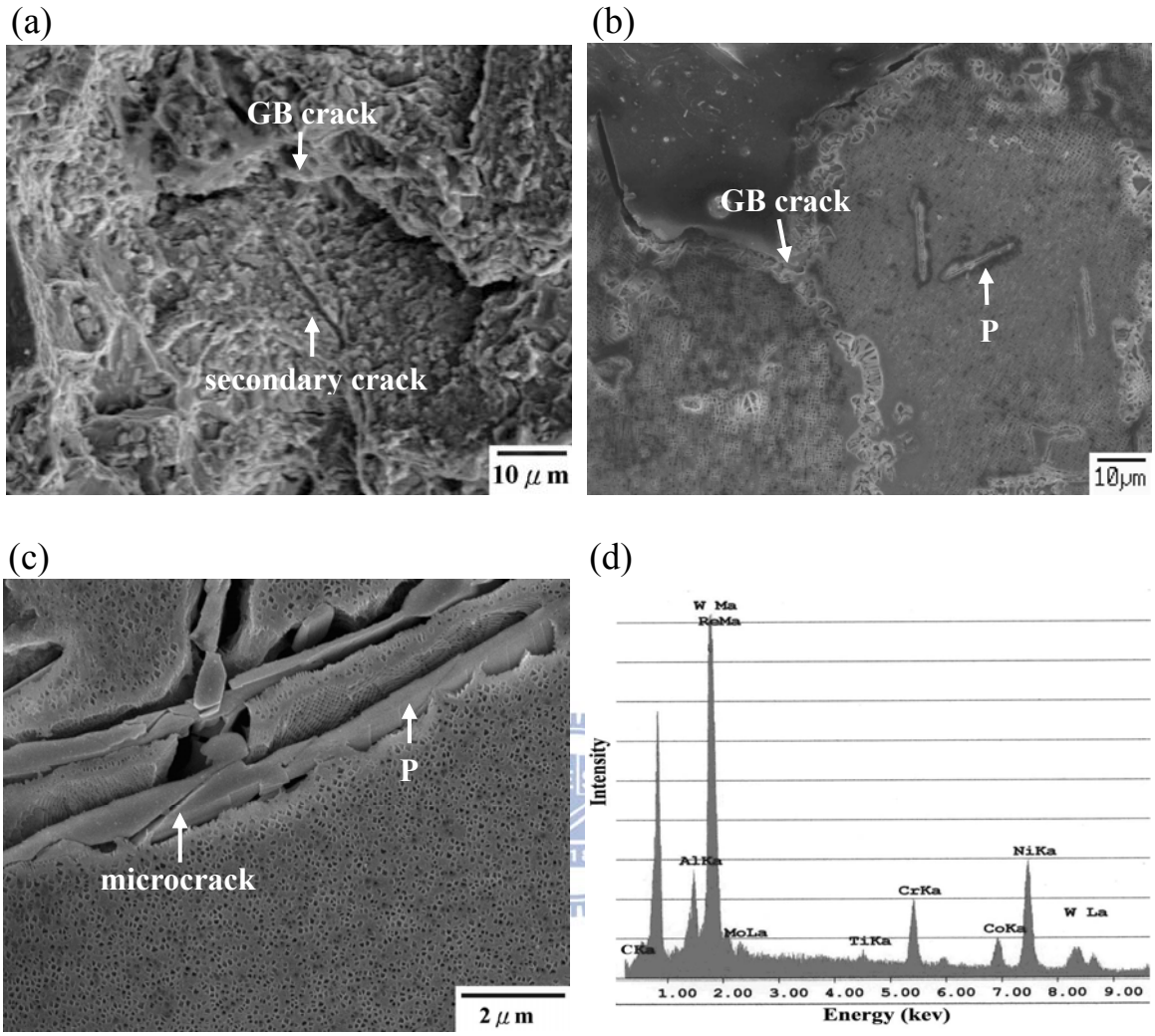

Figure 4.7 Fractographs of the alloy D(5Re) after RT tensile test. (a) Fracture surface, (b) longitudinal section (crack occurs at grain boundary), (c) longitudinal section (microcrack occurs at P phase and P/γ interface), and (d) EDS spectrum at P phase.

(a)

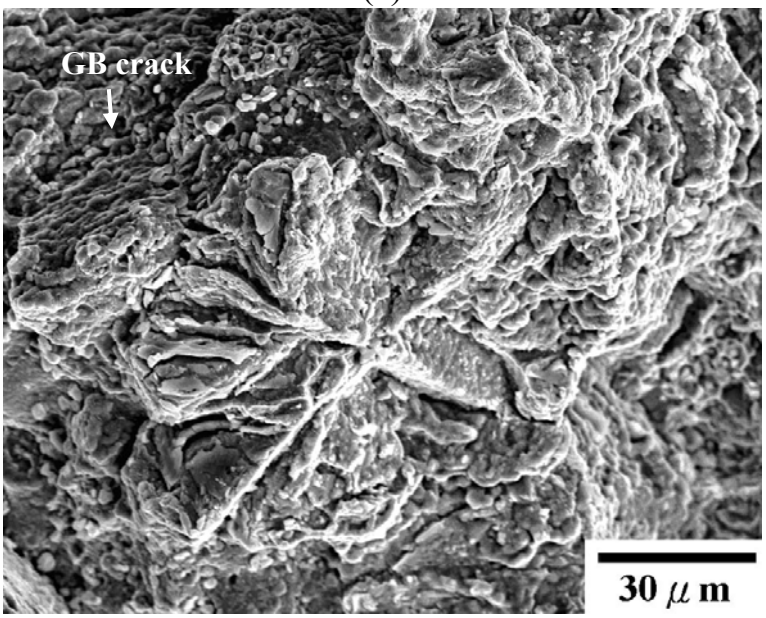

(b)

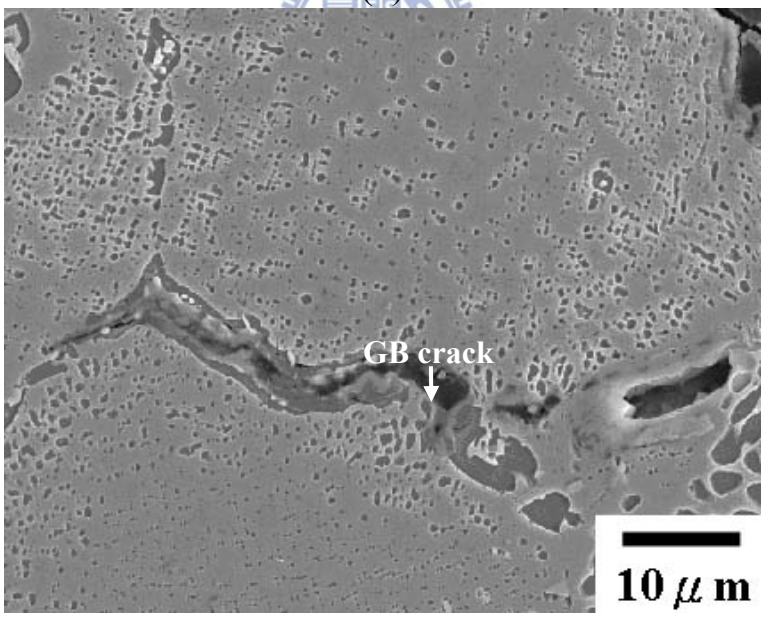

Figure 4.8 Fractographs of the alloy C(3Re) after creep test under 760°C/724MPa. (a) Fracture surface and (b) longitudinal section.

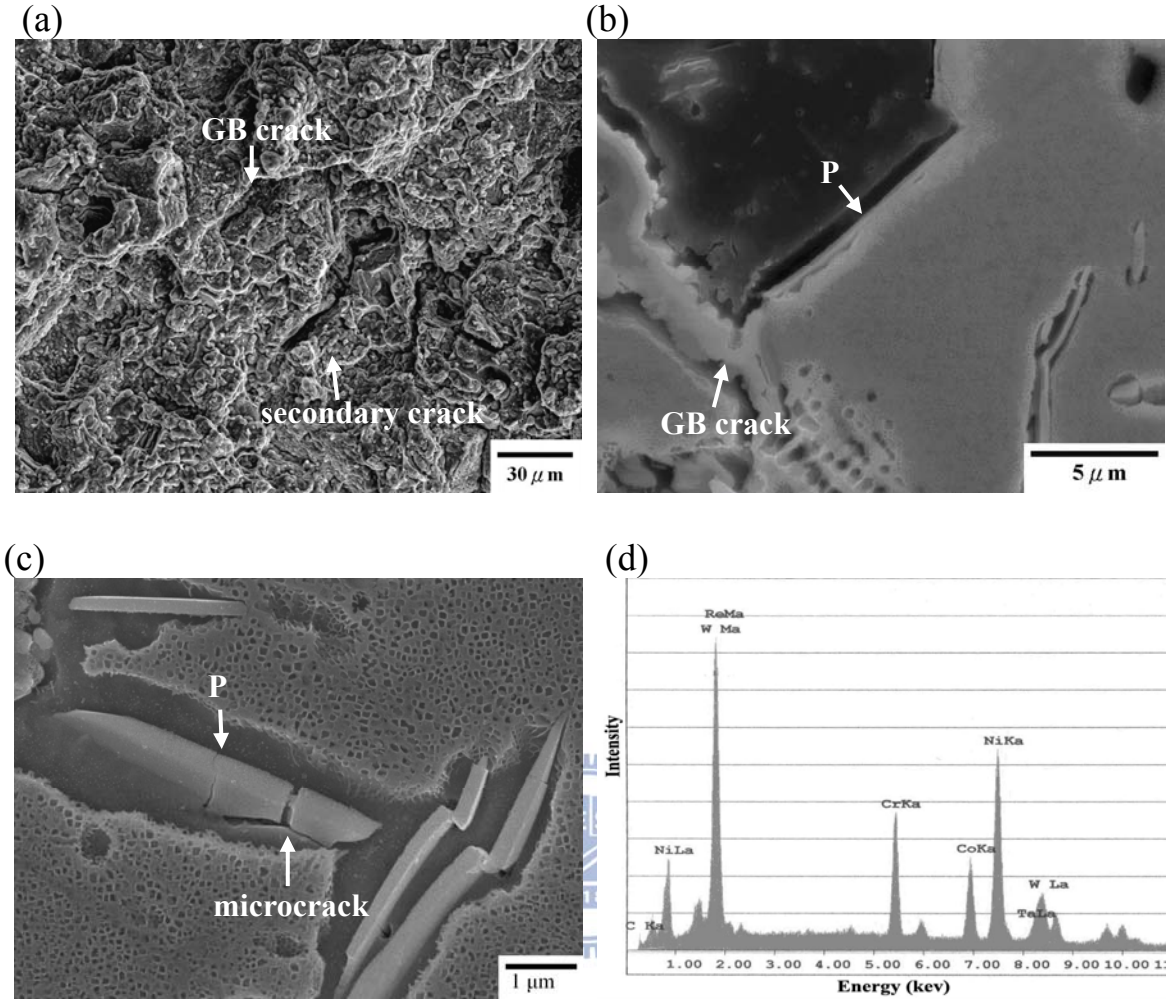

Figure 4.9 Fractographs of the alloy D(5Re) after creep test under 760°C/724MPa. (a) Fracture surface, (b) longitudinal section, (c) longitudinal section (microcrack occurs at P phase and P/γ interface), and (d) EDS spectrum at P phase.

Chapter 5.

Influence of Rhenium on the Grain Boundary Strength, Phase Evolution, and High Temperature Mechanical Properties of a Fine-Grain Nickel-Base Superalloy at 982°C

Influence of Rhenium on the Grain Boundary Strength, Phase Evolution, and High Temperature Mechanical Properties of a Fine-Grain Nickel-Base Superalloy at 982°C

5-1 Introduction

Mar-M247 Ni-base superalloy has been widely employed in fabricating advanced turbine blades and rotating parts in the aerospace industry because of its excellent castability and high temperature properties [9-11]. Because the fine-grain microstructure has advantages such as refined grains, carbides and precipitates, the fine-grain process was developed to improve the strength, creep and fatigue life of integral casting working at intermediate temperature (427~760°C) [24, 46]. Due to superior alloy design and control of the microstructure of Mar-M247 superalloy, the fine-grain integral casting of this material has been applied at temperatures of up to 982°C [18]. Basically, Mar-M247 superalloy consists of 60% volume fraction of the reinforcing precipitates γ′ in a face-centered cubic (FCC) γ matrix [10-11].

In modern Ni-base superalloys, the γ′ phase is limited to approximately 65-70% volume fraction to maximize precipitation hardening [19-20]; hence, the volume fraction of γ′ in Mar-M247 superalloy is nearly at its limit. Strengthening the solid solution of the γ matrix is one way to further improve the strength of this alloy. On the other hand, the reliability of γ′ at elevated temperatures is another concern for Mar-M247 superalloy, because the growth of γ′ significantly degrades creep life. The addition of slow diffusing elements into the alloy to prevent the γ′ coarsing is thought to be a desirable solution to

overcome these detrimental effects. Additionally, the grain boundary strength declines drastically at high temperatures (above 760°C). Therefore, the carbides precipitating at the grain boundary play an important role in the strengthening of grain boundary at high temperature. Through the inhibition of grain boundary sliding, grain boundary carbides contribute to an increase in strength and ductility [9-11].

Current single crystal Ni-base superalloys are heavily alloyed with Re, resulting in increased strength and creep resistance, due to solid solution strengthening and the prevention of γ′ coarsening during thermal exposure [30-35]. The incorporation of higher Re content is restricted by the formation of topological closed-packed (TCP) phases, such as σ, P, μ, and R [13-14, 17, 36]. Formation of a brittle TCP phase is often associated with the deterioration of tensile strength and creep damage [22-23]. To prevent the formation of a TCP phase, controlling the content of Re is an important consideration in the design of superalloys.

Until now, studies have focused on adding Re to single crystal Ni-base superalloys, and the resulting behavior at high temperatures. However, few studies have reported on the effects of adding Re to fine-grain superalloys. The purpose of this investigation was to determine the influence of Re on the mechanical properties of fine-grain Mar-M247 superalloy at 982°C

5-2 Results

5-2-1 Microstructures and characteristics of grain boundary carbides

Figure 3.1 displays the grain size of four alloys following heat treatment. The grain size of alloys refines from 90μm to 50μm with increasing Re content. Figure 5.1a shows the original Mar-M247 superalloy. The main phases comprise: (1) the γ matrix, (2) the reinforcing phase γ′ homogeneously distributed throughout the γ matrix, (3) strip-like and blocky MC carbides within a grain interior, (4) particle and blocky carbides at the grain boundary, and (5) a rosette structure of γ-γ′eutectic. For alloys B(1Re) and C(3Re), the microstructure revealed similar characteristics to that of alloy A(0Re). Alloy D(5Re) exhibited inhomogeneously distributed γ′ phase with fine cuboid shaped γ′ particles in the core area of the grain and the large, block shaped γ′ particles (1–3μm in size) situated in the region near the grain boundary (Figure 5.1b). Needle-like 10–20 μm long P phases were observed within the grain interior in alloy D(5Re), and EDS measurements indicated that this phase had high Re and W contents (Figure 5.1c). Figures 5.2a-c illustrate the characteristic changes in grain boundary carbides. For alloy A(0Re), carbide size ranged from 0.3 to 10μm non-uniformly distributed along the grain boundary. For alloys C(3Re) and D(5Re), the carbides become homogeneous and are more closely distributed in the grain boundary with sizes ranging from 0.5 to 2μm. The EDS measurements indicated that grain boundary carbide of alloy D(5Re) had high Re and W contents (Figure 5.2d). Quantitative statistical results concerning grain boundary carbide characteristics in Mar-M247 superalloy with various proportions of Re are shown in Figure 5.3. Figure 5.3a illustrates that the average particle size of grain boundary carbide is reduced to 1.1μm from 1.9μm in the alloy A(0Re) (i.e., the grain boundary carbides are refined through the addition of Re). Figure 5.3b

shows the linear density of grain boundary carbides along the grain boundary. It is obvious that the number of grain boundary carbides increase with an increase in the addition of Re. This provides evidence that the addition of Re causes an increase in the distribution density. Figure 5.4 shows the highly magnified SEM morphology of γ′ precipitates with two distinct sizes in the core area of grain. Two distinct sizes γ′ phases (primary block γ′ and secondary γ′ phases) were distributed in the alloy A(0Re). The primary γ′ phase becomes finer and more cuboidal with an increase in the content of Re. The sizes of primary block γ′, primary cube γ′**,** and secondary γ′ were about 0.8, 0.3, and 0.05μm, respectively. No obvious difference change in size occurred for secondary γ′ phases in any of alloys.

5-2-2 Tensile and creep tests

Table 5.1 shows the tensile properties of Mar-M247 superalloy with various Re content at room and elevated temperatures. According to the results, the tensile properties of alloys exhibited a similar tendency at various temperatures. The ultimate tensile strength (UTS) and 0.2% offset yield strength (YS) increase with Re content up to a maximum of 3 wt.%. The elongation (El) was nearly invariable in alloys containing 0~3 wt.% Re; however, C(5Re) displayed the lowest of El.

Figure 5.5 illustrates the creep curves of Mar-M247 superalloy with various Re content at 982°C/200MPa condition. Table 5.2 lists the creep data. The creep curves of alloy A(0Re), B(1Re), and C(3Re) showed a steady-state creep stage, followed by an accelerating creep stage leading to failure; however, no primary creep stage was observed. On the other hand, there was no clear definition of steady-state creep regimes for alloy D(5Re); this alloy exhibited a continuing increase in creep rate until failure. According to the EMS-55447 specification

[48], the creep life of the Mar-M247 superalloy should be longer than 25h and the El must exceed 4% at 982°C/200MPa. During service, turbine blades are usually strained below 1 or 2%, therefore the criterion time to reach 1% ($t_{1\%}$) or 2% ($t_{2\%}$) strain was chosen as a key indicator for creep strength [11, 33]. Except for the alloy D(5Re), the creep life and El of alloys A(0Re), B(1Re), and C(3Re) all exceed specification values. The $t_{1\%}$, $t_{2\%}$, period of steady-state, period of accelerating creep, and creep life increased with an increase in Re content, to a maximum at 3 wt.%. In contrast to alloy A(0Re), the $t_{1\%}$, $t_{2\%}$, and creep life of alloy C(3Re) was prolonged by 3.3, 3.1, and 2–3 times, respectively. Finally, the creep properties of alloy D(5Re) decreased from the maximum values attained by the alloy C(3Re), showing the detrimental effect of excessive addition of Re in the alloy.

5-2-3 Fractographic observation and microstructural evolution

To investigate the effect of Re addition on fracture behavior during tensile and creep tests, we examined both the fracture surfaces and the longitudinal sections adjacent to the region of the fractures. Figure 5.6-7 shows the fractographs of 982°C tensile tests. From the fracture surface of alloy A(0Re), it is clear that crack mainly occurs along the grain boundary (Figure 5.6a). Figure 5.6b shows further evidence; a carbide film of approximately 1μm in thickness presents at the fracture position of the grain boundary, indicating a typical intergranular fracture. A similar fracture is seen in alloys B(1Re) and C(3Re), where crack occurs along the grain boundary. The fracture surface of alloy D(5Re) illustrates that the crack is along the grain boundary, and that a secondary crack occurs within the grain interior (Figure 5.7a). Further examination of the longitudinal section shows that the crack is along the P/γ interface whilst the micro-cracks appear at the P phase (Figure 5.7b). The dimensions of the needle-like P phase

are very similar in size to the length of the secondary crack observed in Figure 5.7a. Obviously, another crack onset occurs at the P/γ interface and P phase. In a comparison of the as-heated sample with the fractured sample, no microstructural evolution was observed in the tensile test. In tests of other temperatures, each alloy had the same fracture mode as in the 982°C tests.

For the 982°C/200MPa creep tests, each alloy presented similar fracture behavior as those observed in the tensile test. The fracture surface and longitudinal section of alloy A(0Re) show that cracks occur mainly along the grain boundary, indicating a typical intergranular fracture (Figs. 5.8). Similar fracture behavior is shown in alloys B(1Re) and C(3Re). For the fracture surface of alloy D(5Re), cracks were observed on the grain boundary, and secondary cracks were observed within the grain interior (Figure 5.9a). It is evident from Figure 5.9b that the cracks occurred on the grain boundary, and along the P/γ interfaces. The needle-like P phase showed similar dimensions to the secondary cracks observed in Figure 5.9a. Figures 5.10a-c show the γ′ rafting microstructure in creep failure samples. The primary γ′ phase has directionally coarsened into rafts in the direction perpendicular to the stress axis. No secondary γ′ phase was observed. The alloy A(0Re) exhibited γ′ rafts with varying levels of development and thickness, and finer γ′ tended to raft better than coarse γ′. On the other hand, except for the large γ′ phases existing near the grain boundary exhibited an immature γ′ raft morphology in alloy D(5Re), a higher Re content alloy exhibited a finer and more uniform thickness in the γ′ raft. As Re content increases, average γ′ raft spacing decreases from 0.3 to 0.15μm. To study the evolution of γ′ precipitates, the test was interrupted at creep for 10h. Figure 5.10d provides evidence that the well-developed γ′ rafts have already formed at early stages of creep in the core area of the grains in alloy D(5Re).

5-3 Discussion

5-3-1 Effect of Re content on tensile properties

Generally, the refinement of γ′ size is beneficial to tensile strength. Studies have reported that the large atomic radius of Re partitioned mainly to the γ matrix increases the γ/γ′ lattice misfit, improving the strength of γ matrix [19, 32]. According to the fractographic analysis, intergranular fracture exists in 0~3% wt. Re-containing alloys, indicating the grain boundary strength dominates the tensile strength and fracture behavior over other factors (γ′ size or strength of γ matrix). Generally, grain boundary strength is related to grain size and grain boundary carbide. Except for high temperatures (over the half of melting temperature), a reduction in grain size is beneficial to grain boundary strength [54]. Moreover, finer particles of grain boundary carbide are more beneficial for grain boundary strengthening and for inhibition of grain boundary sliding and cracking [9-10]. Additionally, the fractographic analysis shows that the cracks not only occur along the grain boundary, but also initiate and propagate along the P/γ interface or at the P phase in the alloy D(5Re), indicating that the presence of the needle-liked P phase increases likelihood of another source of crack. Moreover, the formation of P phases results in a decrease in solution-strengthening metal contents (e.g. W and Re) within the matrix. As discussed above, an optimum Re content of 3 wt.% provides optimum tensile properties between conflicting factors of grain boundary strength, γ′ size**,** strength of γ matrix, and P phase.

5-3-2 Effect of Re content on the creep behavior and microstructural evolution

At high temperature, creep behavior was also determined by γ′ size, strength of γ matrix, and grain boundary strength. Most studies show that a cuboidal γ′ with a size of ~0.1–0.5 μm, provides the best creep strength [53, 40]. In this study, the amount of primary cuboidal γ′ phase, of optimum particle size, increased with an increase in the content of Re, to benefit of creep strength. However, adding excessive Re to the alloy, as the alloy D(5Re), caused an in-homogeneous distribution of γ′ phase. The large γ′ phase (1–3 μm in size) existing in the region near the grain boundary was detrimental to creep strength. On the other hand, most studies have reported large atomic radius Re partitions heavily to the γ matrix, increasing γ/γ′ lattice misfit and strength of γ matrix, thereby hindering dislocation motion, resulting in an improvement in creep strength [31, 55]. Additionally, the evolution of γ′ rafting was another major factor in determining creep behavior under high-temperature/low-stress conditions. The γ/γ′ lattice misfit has a tendency to form cuboidal γ′ phases, whereas a spherical γ′ phase was observed for a near-zero γ/γ′ lattice misfit [43]. The negative γ/γ′ lattice misfit, caused by Re partitions in the γ matrix, provided the driving force for the formation of γ′ rafts perpendicular to applied tensile stress [43]. The γ′ rafting impeded the creep deformation by reducing the number of vertical (parallel to the direction of stress) γ channels [56]. It has been reported that γ′ rafts are formed in the early stages of high temperature creep deformation, preventing dislocations to glide or climb [56-57]. Furthermore, narrower γ′ raft spacing is more resistant to dislocation movement [56]. In this study, the γ′ raft microstructure provided evidence that the development of γ′ rafts has already finished in the early stages of creep (Figure 5.10d), and that γ′ raft spacing tended to decline with an increase in Re content in the alloy (Figs.

5.10a-c). Although alloy D(5Re) showed a well-developed γ′ raft microstructure in the core area of the grain, the large γ′ phase existing near the grain boundary was detrimental to creep. The large γ′ phases made it difficult for γ′ rafts to form, due to their near spherical shape with a near-zero γ/γ′ lattice misfit [43]. It must be emphasized that the secondary γ′ phase was too small to resist the movement of dislocation. Moreover, the secondary γ′ phase dissolved during creep. Therefore, the primary γ′ played a more important role than the secondary γ′ as a determinant of creep strength. In summary, a decrease in steady-state strain rate with Re content up to 3 wt.%, suggests that optimizing Re addition could improve steady-state creep resistance by inhibiting the movement of dislocation in three ways: (1) increasing the amount of primary cuboidal γ′ phase, (2) increasing strength of γ matrix, and (3) promoting development of γ′ rafts.

In creep tests, strain hardening was opposed by increases in the stress associated with a reduction in cross-sectional area, and by recovery (due to dislocation climb and the subsequent annihilation of dislocations) [58-59]. In this manner, the steady-state creep strain rate remained constant due to a balance among strain hardening, a reduction in the cross-section of the specimens, and recovery. In this study, 0~3 wt.% Re-containing alloys showed steady-state creep regimes in the early stages of creep; however, alloy D(5Re) showed a continuing increase in creep rate, indicating that strain hardening was too low to counter the decrease in the cross-section of the specimen and recovery. The reduction in strain hardening was due to the P phase depleting the solid solution strengthening elements from the γ matrix and to the large γ′ phase with immature γ′ rafts that existed near the grain boundary. The result was a continuing increase in creep rate seen in the early creep stage of alloy D(5Re). It was noticed that more than approximately 1% strain in any of the alloys, accelerated the strain rate to failure. During this accelerated creep stage, a

remarkable reduction in the cross-sectional area of the specimens resulted in a continual increase in the stress of the gage section, and consequent acceleration in the strain rate to failure. It has been proven that highly localized deformation in the vicinity of the fracture surface is responsible for a rapid increase in creep strain rate [56]. Thus, once the critical strain has been reached, the necking phenomenon dominates the behavior of accelerating creep stage. In our research, most of the cracks existed in the necked zone. This was evidence that the cracks probably initiated and propagated during the accelerating creep stage. Intergranular fractures occurred in the alloys containing 0~3 wt.% Re, and the period of the accelerating creep increased with the content of Re up to 3 wt.%, indicating that Re addition was sufficient to prevent cracks from propagating at the grain boundary. It is interesting to note that the creep life, even the period of accelerating creep stage, was not reduced by grain refinement as Re content was increased to 3 wt.%. The reason was that the presence of small and dense grain boundary carbides prevented cracks from growing along the grain boundary, resulting in an extension of the accelerating creep stage and creep life. Fractographic observations showed that, for alloy D(5Re), the cracks were along the grain boundary and along the P/γ interface—adding another source for carking. The needle-like P phase acts as a barrier for moving dislocations. Dislocations accumulated easily along the P/γ interface, leading to incoherence, and causing the appearance of interfacial cracking [55]. Therefore, the presence of the needle-liked P phase accelerates creep to fracture.

5-4 Conclusions

The following conclusions can be drawn from this work:

1. Quantitative statistical analysis showed a decrease in the size of grain boundary carbides and an increase in the number of grain boundary carbides as Re content in Mar-M247 superalloy was increased. This grain boundary carbide evolution is conducive to the promotion of grain boundary strength.
2. The tensile tests showed that both UTS and YS increased with an increase in Re content up to a maximum of 3 wt.%. The small and dense grain boundary carbides prevented the propagation of cracks contributing to the improvement of tensile strength. A decrease in tensile properties of alloy containing 5 wt.% Re was caused by the formation of needle-like P phase.
3. The 982°C/200MPa creep tests showed that creep life increased with an increase in Re content up to a maximum of 3 wt.%. The creep life of alloys with 3 wt.% Re was extended by 2–3 times that of Re-free alloy. Adding 1~3 wt.% Re reduced the steady-state creep rate and postponed the onset of the acceleration stage in three ways: (1) increasing the amount of primary cuboidal γ′ phase, (2) increasing strength of γ matrix, and (3) promoting the development of γ′ rafts. An increase in the duration of the accelerated creep stage was caused by small and dense grain boundary carbides preventing cracks from propagating along the grain boundary, resulting in the prolongation of the accelerating creep stage. The above mentioned factors resulted in a prolongation of creep life. The formation of needle-like P phase, which increased creep rate to failure, was the major cause of the degradation of creep properties in alloy D(5Re).
4. Cracks initiated and propagated along the grain boundary in Mar-M247 superalloy with 0~3 wt.% added Re in tensile and creep tests. Cracks initiated

and propagated along both the grain boundary and P/γ interface in alloy D(5Re).

Table 5.1 Tensile test results at various temperatures.

Temp.	Alloy	UTS (MPa)	YS (MPa)	El (%)
RT	A(0Re)	1121 - 1139	967 - 987	4.8 - 6.0
	B(1Re)	1124 - 1143	973 - 995	4.7 - 6.2
	C(3Re)	1190 - 1217	1043 - 1074	4.0 - 6.0
	D(5Re)	1083 - 1108	932 - 968	1.3 - 3.0
427°C	A(0Re)	1161 - 1189	973 - 1004	5.2 - 6.7
	B(1Re)	1169 - 1196	982 - 1025	4.5 - 6.9
	C(3Re)	1241 - 1266	1064 - 1095	4.7 - 6.6
	D(5Re)	1087 - 1119	946 - 969	1.5 - 2.7
760°C	A(0Re)	1146 - 1176	969 - 1013	4.4 - 6.0
	B(1Re)	1157 - 1183	985 - 1015	4.5 - 6.3
	C(3Re)	1228 - 1254	1066 - 1088	4.3 - 6.7
	D(5Re)	1071 - 1092	936 - 970	1.7 - 2.9
982°C	A(0Re)	590 - 613	436 - 458	6.4 - 7.5
	B(1Re)	599 - 625	457 - 476	6.2 - 7.1
	C(3Re)	628 - 646	494 - 518	5.5 - 6.2
	D(5Re)	558 - 581	435 - 456	2.5 - 3.6

Table 5.2 Creep test results of Mar-M247 superalloy with various Re content under 982°C/200MPa.

	creep life (h)	El (%)	*$t_{1\%}$ (h)	*$t_{2\%}$ (h)	*steady-state creep rate (s^{-1})	*period of steady-state creep (h)	*period of accelerating creep (h)
EMS-55447	＞25	＞4	-	-	-	-	-
A(0Re)	34.4 - 46.2	11.4-16.4	14.2	21.7	19.45×10^{-8}	13.6	23.8
B(1Re)	55.8 - 69.7	11.1-14.4	29.1	39.0	9.54×10^{-8}	29.1	26.7
C(3Re)	81.9 - 96.3	9.6 -14.1	46.4	66.6	5.98×10^{-8}	46.1	50.2
D(5Re)	11.1 - 19.1	10.5-14.7	7.7	11.6	-	-	19.1

*The value is base on creep curves of Figure 5.5.

** The period of accelerating creep is defined as the time from the beginning of strain rate (the slope of creep curve) rise to the specimen fracture.

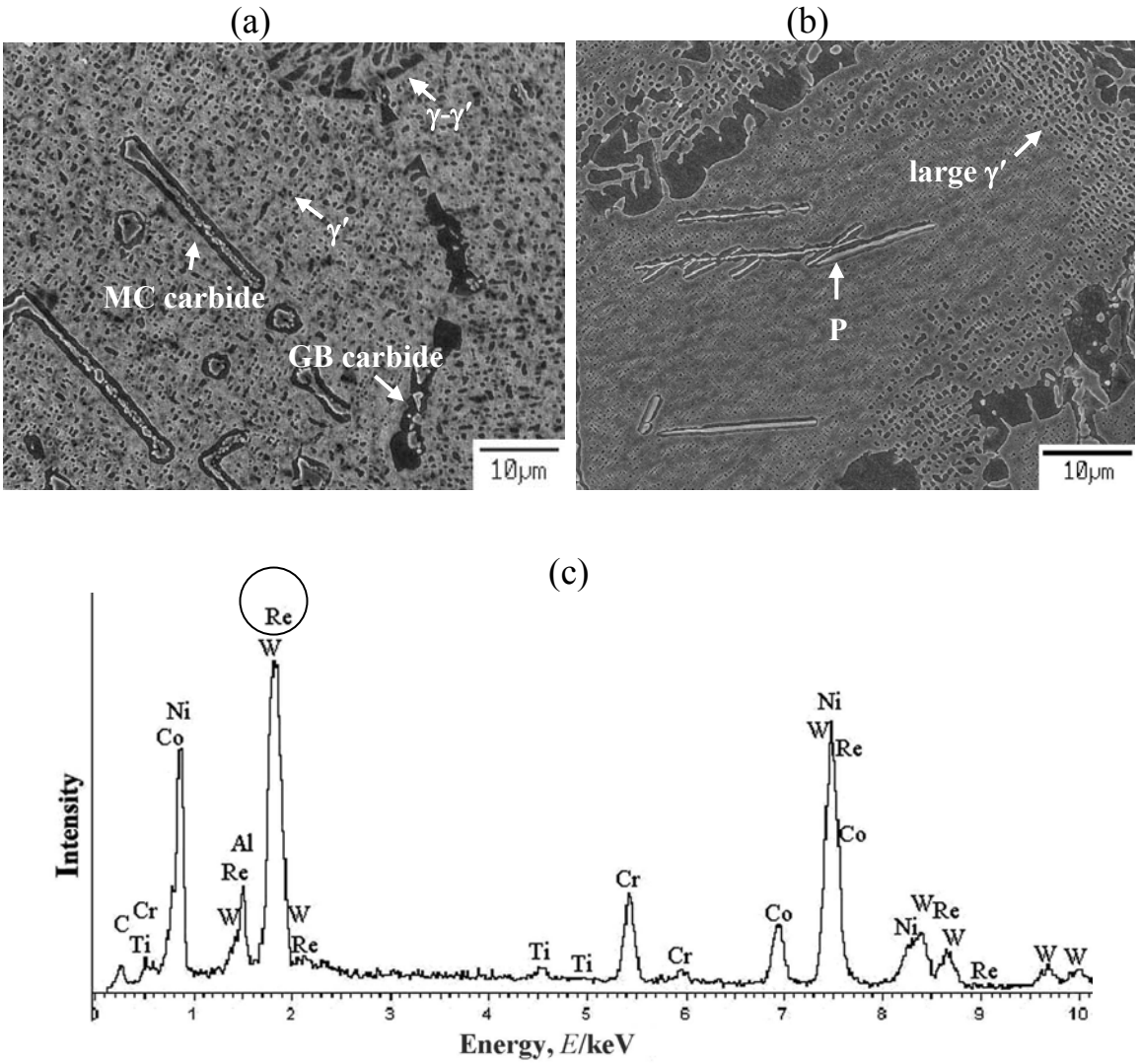

Figure 5.1 SEM microstructures of alloys (a) A(0Re) and (b) D(5Re) after heat treatment. (c) EDS spectrum of TCP phase in alloy D(5Re).

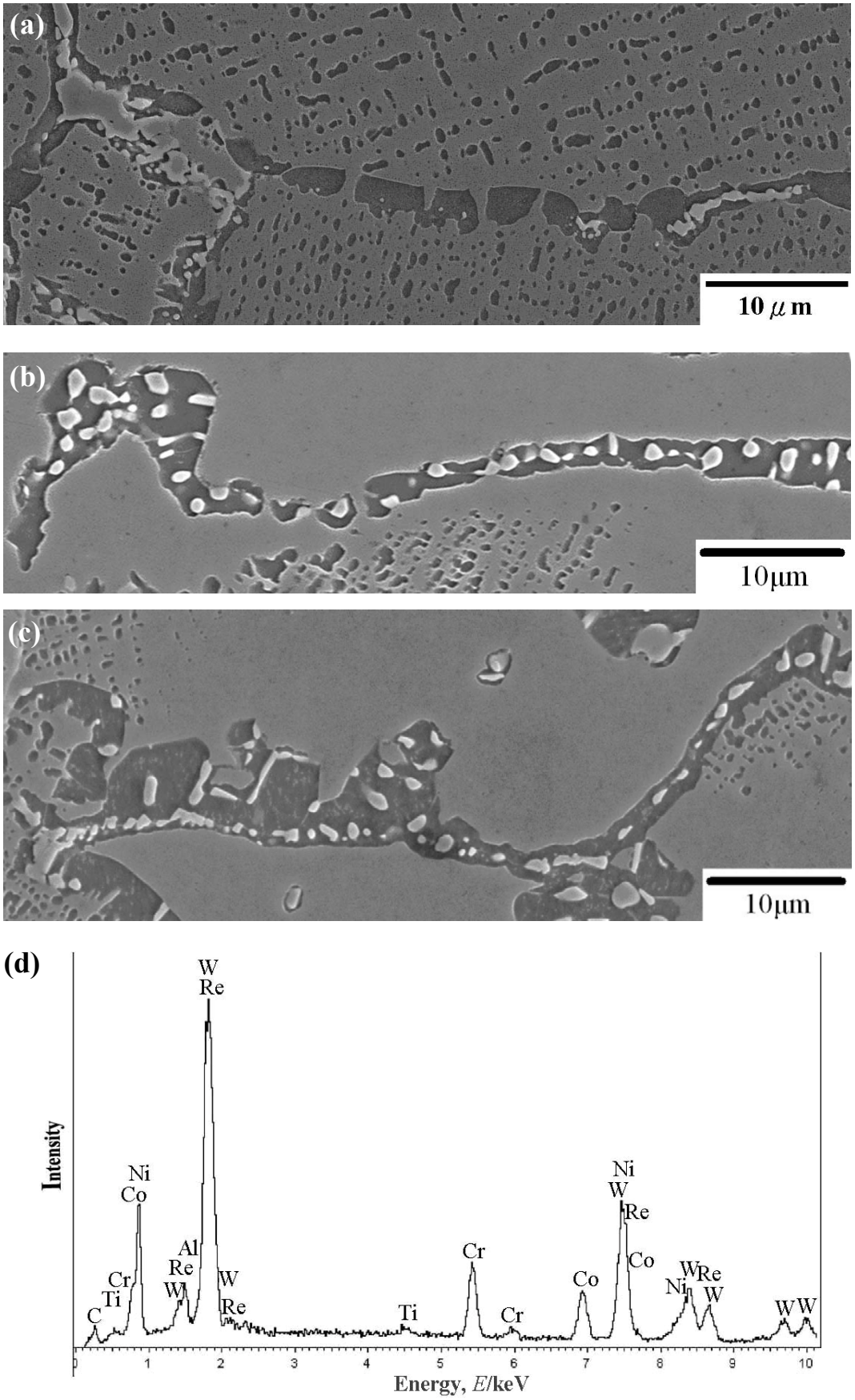

Figure 5.2 Morphology of grain boundary carbides in alloys of (a) A(0Re), (b) C(3Re), and (c) D(5Re); (d) EDS spectrum of grain boundary carbide in alloy D(5Re).

(a)

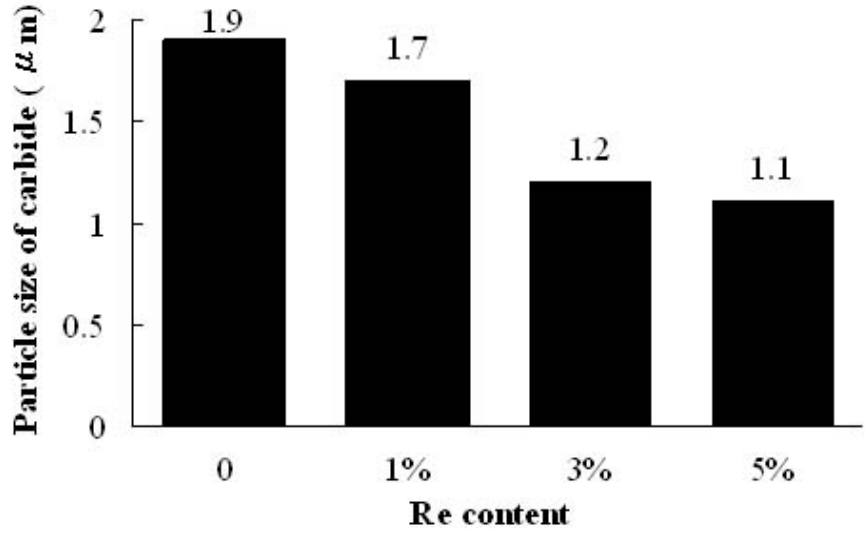

(b)

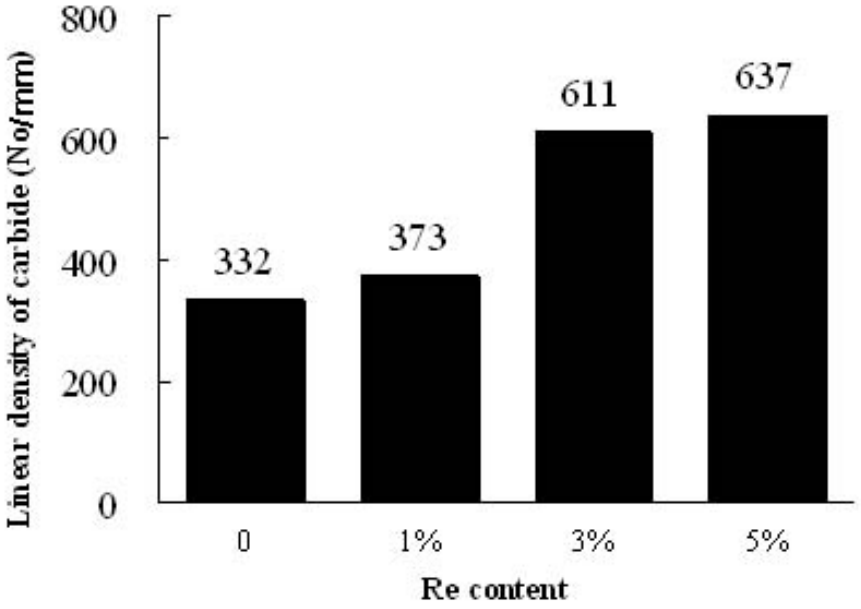

Figure 5.3 Quantitative analysis results of grain boundary carbide characteristics in Mar-M247 superalloy with various Re content, (a) average particle size and (b) linear density of grain boundary carbide.

(a)

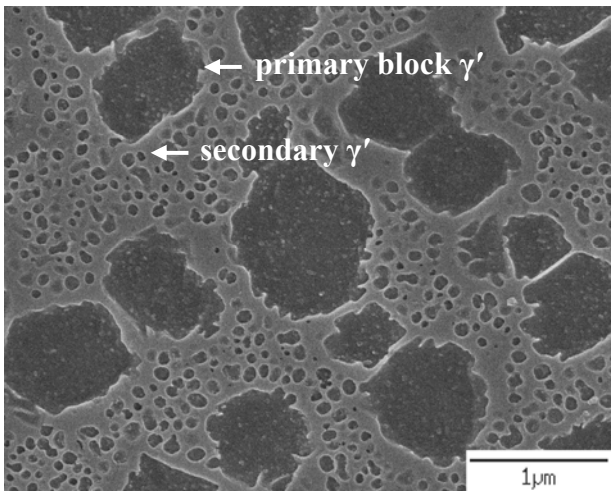

(b)

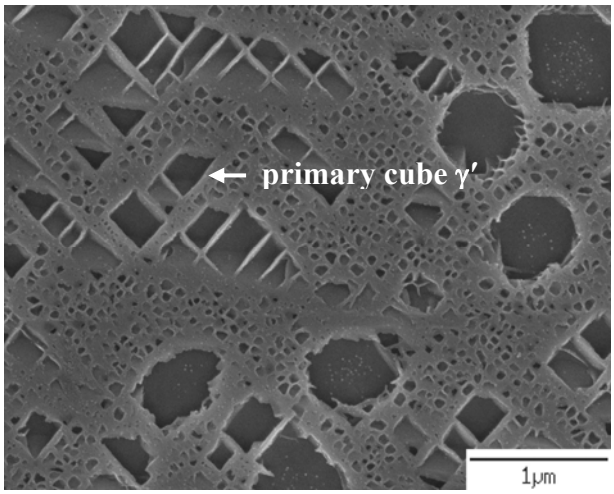

(c)

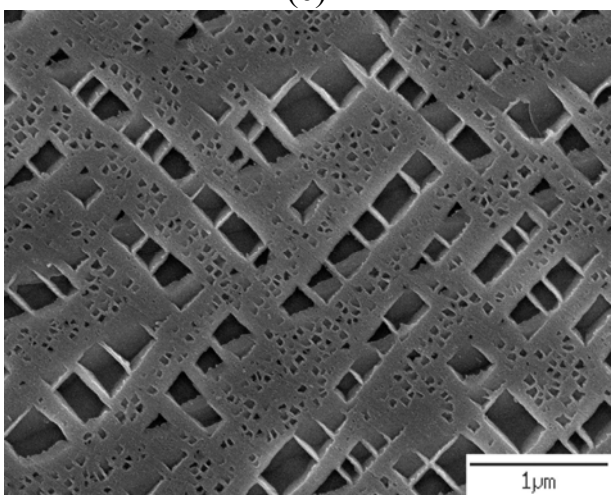

Figure 5.4 γ′ phase morphology (in core area of grain) of alloys (a) A(0Re), (b) C(3Re), and (c) D(5Re) after heat treatment.

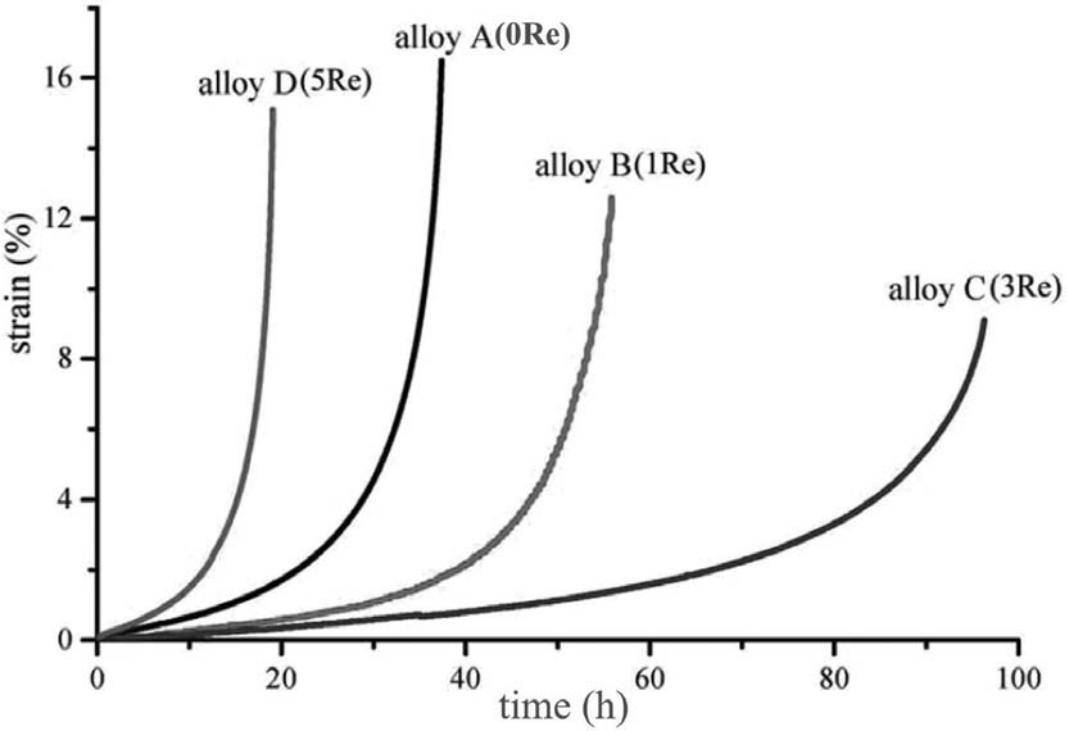

Figure 5.5 Creep curves of Mar-M247 superalloy with various Re content tested under 982°C/200MPa.

(a)

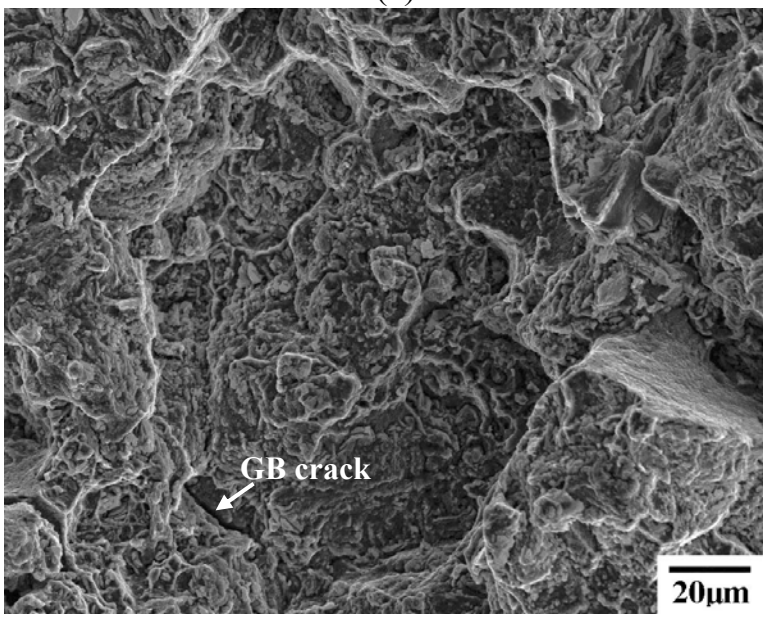

(b)

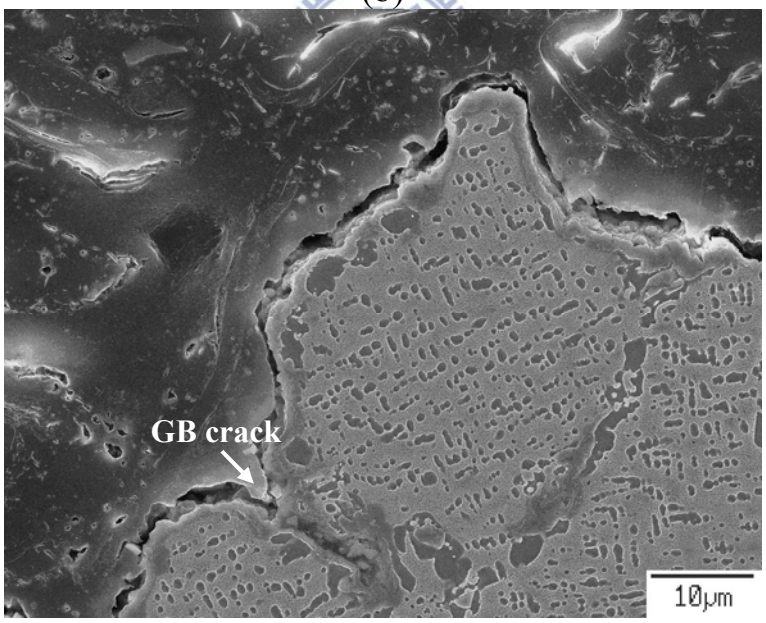

Figure 5.6 Fractographs of the alloy A(0Re) after 982°C tensile test.(a) Fracture surface and (b) longitudinal section.

(a)

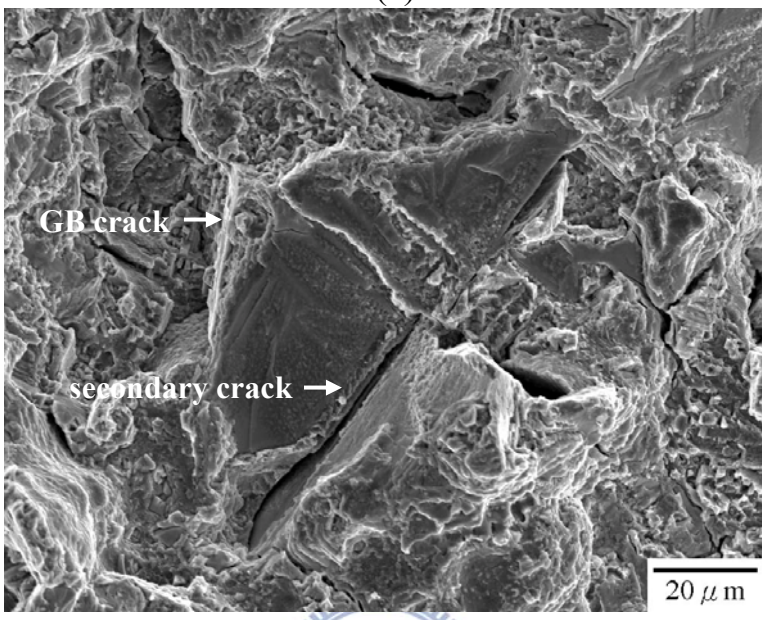

(b)

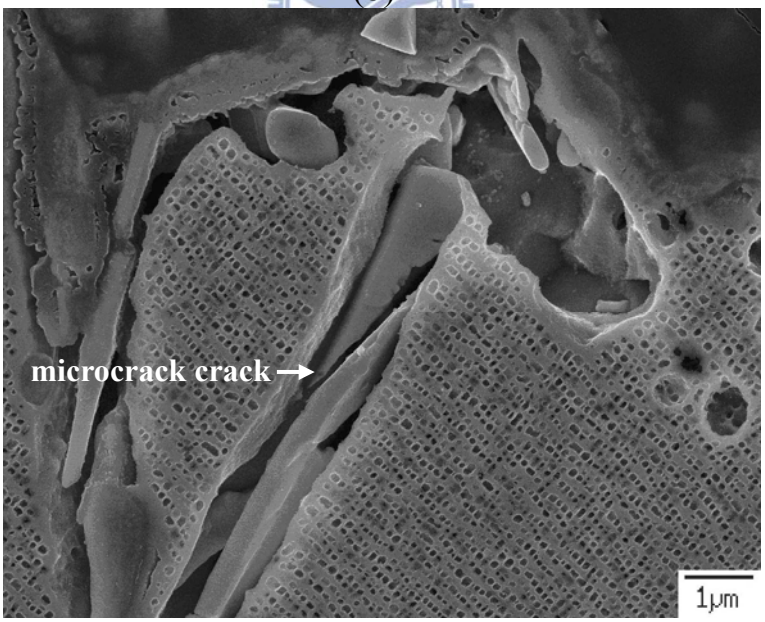

Figure 5.7 Fractographs of the alloy D(5Re) after 982°C tensile test.(a) Fracture surface and (b) longitudinal section.

(a)

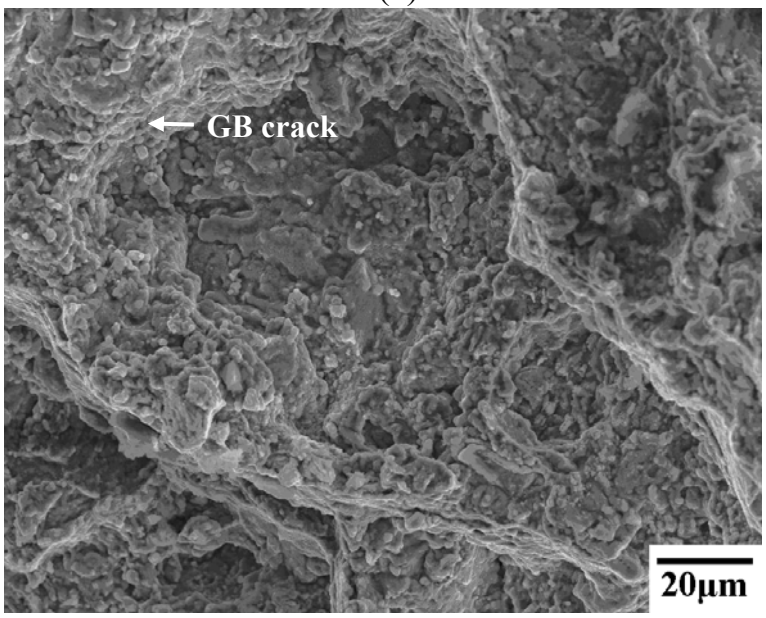

(b)

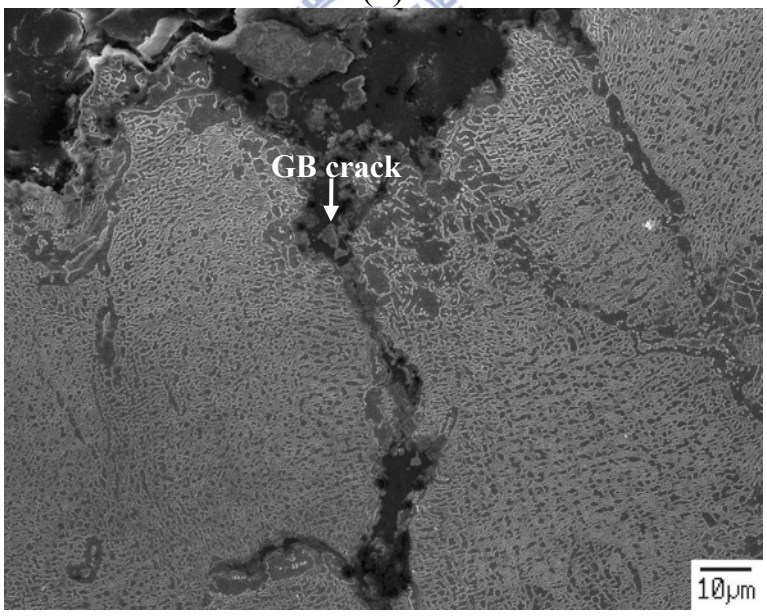

Figure 5.8 Fractographs of the alloy A(0Re) after creep test under 982°C/200MPa creep test. (a) fracture surface and (b) longitudinal section.

(a)

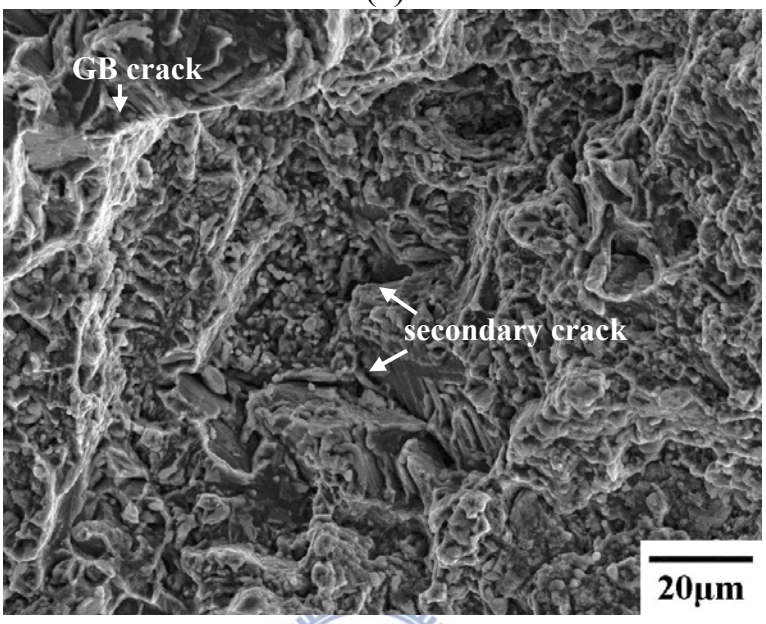

(b)

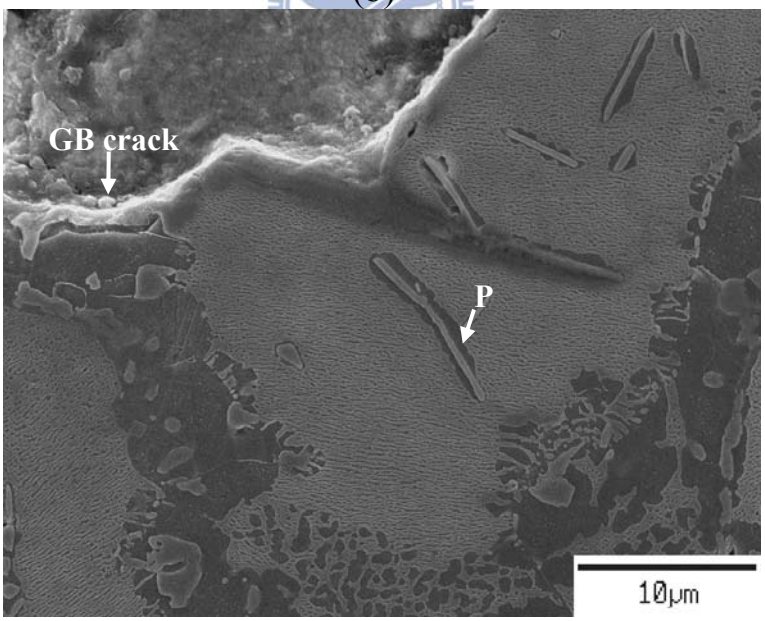

Figure 5.9 Fractographs of the alloy D(5Re) after creep test under 982°C/200MPa creep test. (a) fracture surface and (b) longitudinal section.

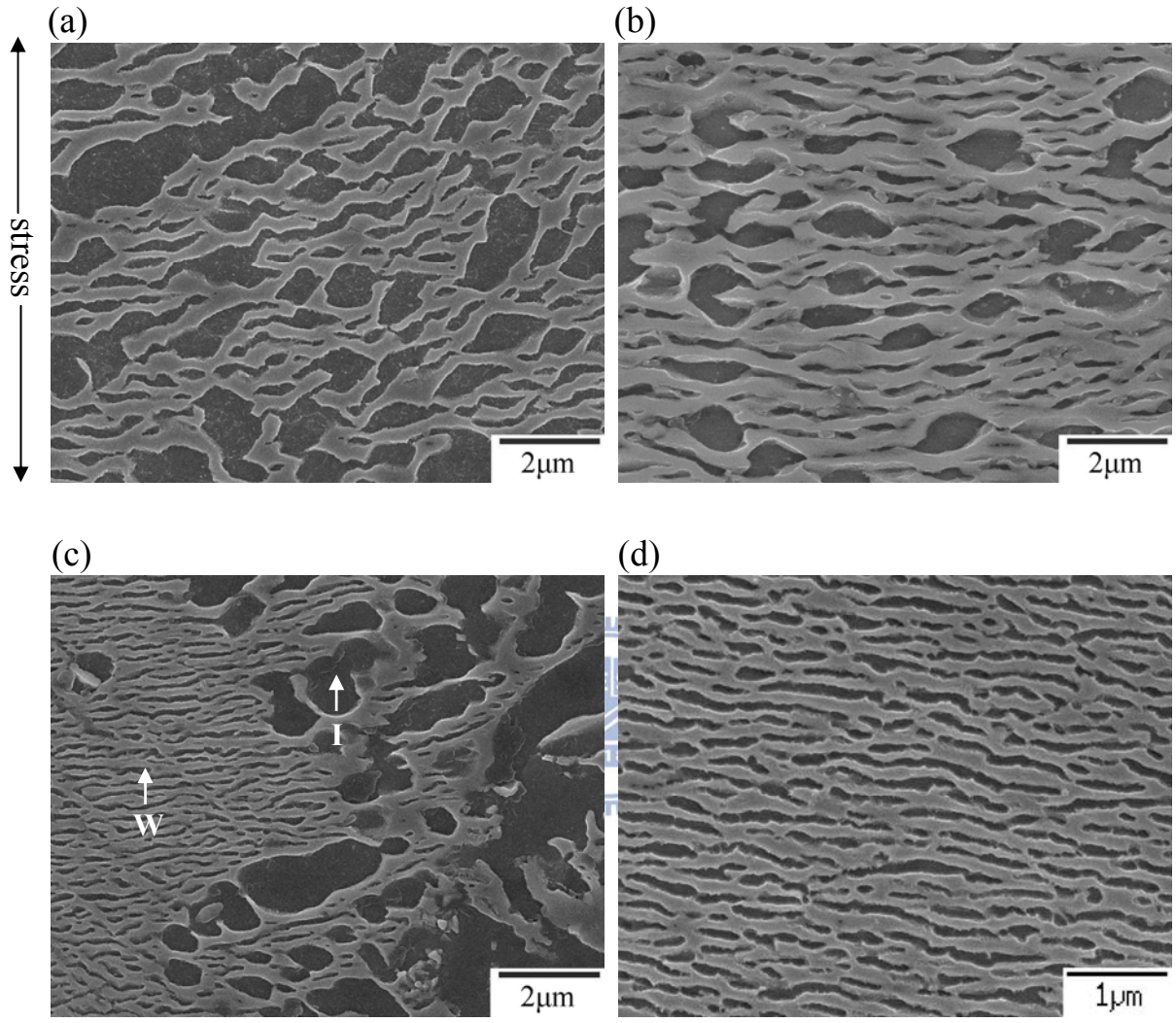

Figure 5.10 γ′ rafting microstructures of alloys (a) A(0Re), (b) C(3Re), and (c) D(5Re) in crept failure sample. For alloy D(5Re), the well-developed γ′ raft exited in core area of grain marked as "W" and immature γ′ raft existed near the grain boundary marked as "I". (d) γ′ rafting microstructure (in core area of grain) of alloy D(5Re) in interrupted creep specimen which was crept for 10h.

Chapter 6.

Summary

Summary

In the present study, the effects of rhenium addition on microstructures and mechanical properties of Ni-base Mar-M247 superalloy have been examined. Based on the experimental results, some conclusions are given as follows:

1. The grain size of the Mar-M247 superalloy with 0, 1, 3, and 5 wt.% Re content was 90, 70, 60, and 50 μm, respectively, indicating that Re addition reduces grain size.
2. The primary γ′ phase becomes finer and more cuboidal as Re content increases.
3. 3 wt.% Re is a critical addition to initiate the formation of the TCP phase and maintain optimal microstructure.
4. With 5 wt.% Re addition, the segregation of Re and W caused phase instabilities that led needle–like P phase to form within the grain interior.
5. Microhardness tests showed that addition of Re could enhance the strength of the γ/γ′ matrix, and the strongest γ/γ′ matrix could be obtained in the alloy with 3 wt.% of Re addition.
6. Quantitative statistical analysis showed a decrease in the size of grain boundary carbides and an increase in the number of grain boundary carbides as Re content in Mar-M247 superalloy was increased. This grain boundary carbide evolution is conducive to the promotion of high temperature grain boundary strength.
7. Cracks initiated and propagated along the grain boundary in Mar-M247 superalloy with 0~3 wt.% added Re in tensile and creep tests. Cracks initiated and propagated along both the grain boundary and P/γ interface in alloy with 5 wt.% added Re.
8. 3 wt.% of Re addition is the optimum concentration for obtaining fine-grain

Mar-M247 superalloy with superior tensile and creep properties at moderate and elevated temperatures.

References

[1] C.T. Sims, N.S. Stoloff, W.C. Hagel, Superalloys II, John Wiley & Sons, New York (1987) pp.3

[2] C.T. Sims, N.S. Stoloff, W.C. Hagel, Superalloys II, John Wiley & Sons, New York (1987) pp.61

[3] C.T. Sims, N.S. Stoloff, W.C. Hagel, Superalloys II, John Wiley & Sons, New York (1987) pp.8

[4] C.T. Sims, N.S. Stoloff, W.C. Hagel, Superalloys II, John Wiley & Sons, New York (1987) pp.66

[5] C.T. Sims, N.S. Stoloff, W.C. Hagel, Superalloys II, John Wiley & Sons, New York (1987) pp.100

[6] C.T. Sims, N.S. Stoloff, W.C. Hagel, Superalloys II, John Wiley & Sons, New York (1987) pp.104-105

[7] C.T. Sims, N.S. Stoloff, W.C. Hagel, Superalloys II, John Wiley & Sons, New York (1987) pp.67-68

[8] C.T. Sims, N.S. Stoloff, W.C. Hagel, Superalloys II, John Wiley & Sons, New York (1987) pp.111-115

[9] H.Y. Bor, C.G. Chao, C.Y. Ma, Metall. Trans. A. 30A (1999) pp.551-561.

[10] H.Y. Bor, C.G. Chao, C.Y. Ma, Scripta. Meter. 38 No. 2 (1998) pp. 329-335.

[11] W.F. Brown, S.J Setlak, Aerospace structural Metals Handbook, thirty ninth ed., Vol. 6, (1999) Code 4218

[12] C.T. Sims, N.S. Stoloff, W.C. Hagel, Superalloys II, John Wiley & Sons, New York (1987) pp.117-118

[13] C.M.F. Rae, R.C. Reed, Acta Mater., 49 (2001) pp. 4113-4125.

[14] J.X. Yang , Q. Zheng, X.F. Sun, H.R. Guan, Z.Q. Hu, Mater. Sci. Eng. A465 (2007) pp.100-108.

[15] C.T. Sims, N.S. Stoloff, W.C. Hagel, Superalloys II, John Wiley & Sons, New York (1987) pp.420-426

[16] C. N. Wei, H. Y. Bor, Li. Chang, Mater. Sci. Eng. A 527 (2010) pp.3741–3747

[17] L. Liu, T. Huang, Y. Xiong, A. Yang, Z. Zhao, R. Zhang, J. Li, Mater. Sci. Eng. A 394 (2005) pp.1-8.

[18] Allied-Signal Aerospace Company, Garrett Engine Division (1991) Specification No. EMS52508

[19] J.Rüusing, N. Wanderka, U. Czubayko, V. Naundorf, D. Mukherji, J. Rösler, Scripta. Meter. 46 (2002) pp.235-240.

[20] F. Diologent, P. Caron, Mater. Sci. Eng. A385 (2004) pp.245-257.

[21] S. Tin, T.M. Pollock, Mater. Sci. Eng. A348 (2003) pp.111-121.

[22] C.T. Sims, N.S. Stoloff, W.C. Hagel, Superalloys II, John Wiley & Sons, New York (1987) pp. 221-226.

[23] A. Volek, R.F. Singer, R. Buergel, J. Grossmann, Y. Wang, Metall. Trans. A. 37A (2006) pp.405-410.

[24] C. N. Wei, H. Y. Bor, L. Chang, Mater. Trans. 49 (2008) pp.193–201.

[25] H.Y. Bor, C.G. Chao, C.Y. Ma, Metall. Trans. A 31A (2000) pp.1365-1373.

[26] M.V. Nathal, R.D. Maier, L.J. Ebert, Metall. Trans. A 13A (1982) pp.1767-1774.

[27] M.V. Nathal, R.D. Maier, L.J. Ebert, Metall. Trans. A 13A (1982) pp.1775-1782.

[28] Lin Liu, Taiwen Huang, Yuhua Xiong, Aimin Yang, Zhilong Zhao, Rong Zhang, Jinshan Li, Proceedings of the 10th International Symposium on Superalloys, ed. by K.A. Green, T.M. Pollock, H. Harada,T.E. Howson, R.C. Reed, J.J. Schirra, S, Walston, (TMS, Warrendale, PA, 2004) pp.493-500.

[29] C.T. Sims, N.S. Stoloff, W.C. Hagel, Superalloys II, John Wiley & Sons, New York (1987) pp.66-94.

[30] M.V. Acharya, G.E. Fuchs, Mater. Sci. Eng. A381 (2004) pp.143-153.

[31] K. Durst, M. Göken, Mater. Sci. Eng. A387-389 (2004) pp.312-316.

[32] G.E. Fuchs, Mater. Sci. Eng. A300 (2001) pp.52-60.

[33] S. Wöllmer, T. Mack, U. Glatzel, Mater. Sci. Eng. A319-321 (2001) pp.792-795.

[34] A.F. Giamei, D.L. Anton, Metall. Trans. A. 16A (1985) pp.1997-2005.

[35] R. Burgel, J. Grossmann, O. Lusebrink H. Mughrabi, F. Pyczak, R.F. Singer, A. Volek, Proceedings of the 10th International Symposium on Superalloys, ed. by K.A. Green, T.M. Pollock, H. Harada,T.E. Howson, R.C. Reed, J.J. Schirra, S. Walston, (TMS, Warrendale, PA, 2004) pp.25-34.

[36] A.C. Yeh, S. Tin, Metall. Trans. A 37A (2006) pp.2621-2631.

[37] E. V. Monastyrskaia, E. V. Petrov, V. E. Beljaev, A. M. Dushkin, Proceedings of the 10th International Symposium on Superalloys, ed. by K.A. Green, T.M. Pollock, H. Harada,T.E. Howson, R.C. Reed, J.J. Schirra, S. Walston, (TMS, Warrendale, PA, 2004) pp.779-786.

[38] R.A. Hobbs, S. Tin, C.M.F. Rae, R.W. Broomfield, C.J. Humphreys, Proceedings of the 10th International Symposium on Superalloys, ed. by K.A. Green, T.M. Pollock, H. Harada,T.E. Howson, R.C. Reed, J.J. Schirra, S. Walston, (TMS, Warrendale, PA, 2004) pp.819-825.

[39] Robert E. Reed-Hill, Reza Abbaschian, Physcial Metallurgy Principles, (PWS Publishing Company, Bonton, 1994) pp.434-436.

[40] J.S. Hou, J.T. Guo, J. Mater. Eng. Perform. 15(1) (2006) pp.67-75.

[41] P.J. Warren , A. Cerezo, G.D.W. Smith, Mater. Sci. Eng. A250 (1998) pp.88-92.

[42] A. Volek, F. Pyczak, R.F. Singer, H. Mughrabi, Scripta. Meter. 52 (2005) pp.141-145.

[43] L.J Carroll, Q. Feng, J.F. Mansfield, T.M Pollock, Metall. Trans. A 37A (2006) pp.2927-2938.

[44] C.T. Sims, N.S. Stoloff, W.C. Hagel, Superalloys II, John Wiley & Sons, New York (1987) pp.111-116.

[45] C. N. Wei, H. Y. Bor, L. Chang, Mater. Trans. 49 (2008) pp.193-201.

[46] H. E. Huang, C. H. Koo, Mater. Trans. 45 (2004) pp.554-561.

[47] C.T. Sims, N.S. Stoloff, W.C. Hagel, Superalloys II, John Wiley & Sons, New York (1987) pp.98-105.

[48] Allied-Signal Aerospace Company, Garrett Engine Division, Specification (1988) No. EMS55447

[49] C.T. Sims, N.S. Stoloff, W.C. Hagel, Superalloys II, John Wiley & Sons, New York (1987) pp.62-66.

[50] C.T. Sims, N.S. Stoloff, W.C. Hagel, Superalloys II, John Wiley & Sons, New York (1987) pp.78.

[51] Q.Z. Chen, C.N. Jones, D.M. Knowles, Mater. Sci. Eng. A385 (2004) pp.402-418

[52] C.T. Sims, N.S. Stoloff, W.C. Hagel, Superalloys II, John Wiley & Sons, New York (1987) pp.39-40.

[53] C.T. Sims, N.S. Stoloff, W.C. Hagel, Superalloys II, John Wiley & Sons, New York (1987) pp.255-261.

[54] C.T. Sims, N.S. Stoloff, W.C. Hagel, Superalloys II, John Wiley & Sons, New York (1987) pp.91-95.

[55] C.T. Sims, N.S. Stoloff, W.C. Hagel, Superalloys II, John Wiley & Sons, New York (1987) pp.62-63.

[56] R.C. Reed, N. Matan, D.C. Cox, M.A. Rist, C.M.F. Rae, Acta Mater. 47 (1999) pp.3367-3381.

[57] A.C. Yeh, A. Sato, T. Kobayashi, H. Harada, Mater. Sci. Eng. A. 490 (2008) pp.445-451.

[58] R.E. Reed-Hill, R. Abbaschian, Physcial Metallurgy Principles, (PWS Publishing Company, Boston, 1994), pp.881-885.

[59] L.Z. He, Q. Zheng, X.F. Sun, H.R. Guan, Z.Q. Hu, A.K. Tieu, C. Lu, H.T. Zhu, Metall. Trans. A. 36A (2005) pp.2385-2391.

List of Publications

- **國外期刊**

1. **Jian-Hong Liao**, Hui-Yun Bor, Chuen-Guang Chao, Tzeng-Feng Liu, "Effects of Rhenium on Microstructure and Phase Stability of MAR-M247 Ni-Base Fine-Grain Superalloy", published in Materials Transactions, Vol. 51, No.4, 2010, pp.810-817.
2. **Jian-Hong Liao**, Hui-Yun Bor, Chuen-Guang Chao, Tzeng-Feng Liu, "Influence of Rhenium on the Mechanical Behavior and Fracture Mechanism of a Fine-Grain Superalloy at Elevated Temperatures", published in Materials Transactions, Vol. 52, No.2, 2011, pp.201-209.
3. **Jian-Hong Liao**, Hui-Yun Bor, Chuen-Guang Chao, Tzeng-Feng Liu, "Influence of rhenium on the grain boundary strength, phase evolution, and high temperature mechanical properties of a fine-grain nickel-base superalloy at 982°C", published in Materials Transactions, Vol. 52, No.10, 2011, pp.1989-1997.

- **國內期刊**

1. **廖健鴻**, 薄慧雲, 魏肇男, 洪炎輝, 鄭榮瑞, 劉增豐, 林於隆, 鄭文興, "鉿元素對鑄造Mar-M247超合金細晶顯微組織及拉伸性能影響之研究",鑄造工程學刊, Vol. 34, No 3, 2008, pp.13-26.

   (榮獲鑄造學會97年鑄造論文獎)

2. **廖健鴻**, 薄慧雲, 魏肇男, 朝春光, 劉增豐, 林於隆, 鄭文興, "鉿元素對細晶鑄造Mar-M247超合金在760℃下機械性能及破壞模式之影響", 鑄

造工程學刊, Vol. 35, No 3, 2009, pp.1-12.

(榮獲鑄造學會 99 年鑄造論文獎)